THE PENNSYLVANIA STATE UNIVERSITY
SCHREYER HONORS COLLEGE

DEPARTMENT OF MECHANICAL AND NUCLEAR ENGINEERING

SCALED VEHICLE TESTING OF CONTROL ALGORITHMS TO PREVENT VEHICLE ROLLOVER

JANINE M. KOWALCZYK

Fall 2006

A thesis
submitted in partial fulfillment
of the requirements
for a baccalaureate degree
in Mechanical Engineering
with honors in Mechanical Engineering

Reviewed and approved* by the following:

Sean N. Brennan
Assistant Professor of Mechanical Engineering
Thesis Supervisor

Mary I. Frecker
Associate Professor of Mechanical Engineering
Honors Adviser

*Signatures are on file in the Schreyer Honors College.

We approve the thesis of Janine M. Kowalczyk:

Date of Signature

Sean N. Brennan
Assistant Professor of Mechanical Engineering
Thesis Supervisor

Mary I. Frecker
Associate Professor of Mechanical Engineering
Honors Adviser

9-2213-2511

ABSTRACT

Vehicle rollover is a large concern in the automobile industry. It claims many lives each year. Research to investigate the dynamics involved in rollover accidents is necessary in order to mitigate rollover.

This work focuses on an initial investigation of predicting vehicle wheel lift thresholds and determining a means to prevent it. Through simulation and experimental results, road conditions and vehicle parameters that increase rollover susceptibility are explored.

First, vehicle dynamic models are derived to create a better understanding of the physics behind rollover. A two-degree-of-freedom model is compared to a three-degree-of-freedom model for validation of the planar dynamics. The threshold for tire saturation is determined with both models. Then it is juxtaposed with the threshold determined for wheel lift of a vehicle calculated in terms of the maximum restoring moment of the suspension in order to determine if a roll before slip condition exists. The effects of a banked surface on the wheel lift threshold are also established

Second, a feed-forward control method is used to modify the dynamics of a vehicle that is likely to experience wheel lift and hence rollover. By taking the differences in parameters of a more stable vehicle into account, an algorithm is designed to alter the steering input of a vehicle to avert perilous conditions.

Finally, the control algorithm is implemented in an experiment utilizing a scaled vehicle. The vehicle has similar dimensionless parameters to that of an actual vehicle.

Wheel lift is achieved for the scaled vehicle on a banked surface with a sinusoidal steering input and then prevented by the controller at the same conditions.

TABLE OF CONTENTS

LIST OF FIGURES

LIST OF TABLES

ACKNOWLEDGEMENTS

First I would like to thank my family. They have always reminded me that I was capable of accomplishing anything as long as I believed in myself and remained confident in my abilities.

I am also grateful for my advisers at Penn State. I would like to thank Dr. Sean Brennan for supervising my work on this thesis. He is an excellent teacher, and I have learned a great deal from him. He encouraged me to work hard while making the research process enjoyable. He also helped me renew my interest in mechanical engineering by providing a great project to work on and believing in me. I also wish to thank Dr. Mary Frecker for being my reader and providing academic advice throughout my final semesters.

I also owe thanks to everyone in the research group who provided help and support. First and foremost, I would like to thank Sittikorn Lapapong for the long hours he spent helping me collect data and assisting me with the scaled vehicle. I also wish to thank Adam Dean for lifting my spirits and renewing my energy and Vishisht Gupta for his treadmill hardware savvy the morning I was ready to quit. I would also like to thank Bridget Hamblin for her cheerful presence in the lab and her support.

Finally, I am grateful for all of my amazing friends. Life would not be nearly as enjoyable without them, and their continuous support has helped me persevere. I will always remember the good conversations and the great times we enjoyed together. They have certainly been my best defense against stress throughout my time at Penn State.

Chapter 1

Introduction

This thesis will focus on studying the thresholds for wheel lift predicted by vehicle models, developing a control algorithm to modify unsafe steering inputs that might lead to wheel lift, and using a scaled vehicle to test the algorithm's ability to prevent vehicle rollover on a banked road surface. The main goals for this work are to show how a banked surface affects the likelihood of vehicle rollover and to use a control algorithm to mitigate wheel lift on this type of surface.

1.1 Motivation

There are various sources of motivation for this work. The first is to help find a way to make vehicles safer. In order to help prevent vehicle rollover, an understanding of vehicle roll models and the conditions that cause rollover must be explored. Therefore the second source of motivation for this work is to further the knowledge in this area. Finally, exploration of safe and cost efficient methods of vehicle rollover experiments is advantageous to academic research. This work will demonstrate the benefits of using a scaled vehicle instead of a full-size vehicle for controller testing.

1.1.1 Safety Goals of the Automobile Industry

One of the largest concerns of automobile manufacturers is safety. The development of the automobile has made transportation much more feasible for the average person, but the problem of accidents has not been solved. In 2001, more than 42,000 fatal car crashes occurred in the United States [**1**]. It is a common goal to eliminate or at least help prevent this large number of deaths. The U.S. Department of Transportation reports that automotive safety features have saved 329,000 lives since 1960 [**2**]. Commercials often boast that their cars have surpassed safety standards to appeal to customers who are rightfully worried about the wellbeing of their family and friends. According to a poll led by Harris Interactive Inc., six of the top ten most desired features by consumers were safety related [**2**]. Automobile safety will continue to be an issue throughout the years to come.

One of the latest ideas in the automobile industry is the development of crash avoidance systems which have the purpose of helping drivers avoid and prevent accidents before they occur. This is much different than the majority of today's safety features which collaborate to protect the driver and passengers during or after the event of a car crash. Reducing the total number of accidents would consequently reduce the number of fatalities caused by automobiles.

A key challenge in preventing accidents is deciding how to intercede. Driver error causes ninety percent of all crashes [**3**]. Decreasing the amount of driver error would potentially create safer roads. That is why one of the main ideas in industry is to warn the driver in the case of an impending accident or alter the input of the driver before it causes an accident. Unfortunately, the driver reaction times and the limitations of advanced warning systems limit the effectiveness of a driver-centered approach.

Automobile manufacturers are already beginning to provide new automated-assist features that will help prevent collision. For example, both Honda and Toyota have developed systems for this purpose. Honda's system uses radar to detect possible collisions and warns the driver with a buzzer and light on the dashboard. Automation immediately begins to assist the driver as the system tightens the seatbelt and begins to apply the brakes slightly. If the driver applies the brakes, the power of the brakes is strengthened. If the driver seems oblivious, the car will increase its braking and prepare for a crash [**1**]. Toyota, on the other hand, is utilizing a system that activates only when the driver reacts. It also tightens the seatbelt and assists in braking before a crash, but only if the driver responds to the possibility [**1**].

These developments are promising for avoiding or mitigating collision, but what about rollover prevention? For passenger vehicles, 33% of fatalities are caused by rollover crashes even though only 3% of automobile crashes involve rollover [**4**]. Over 10,000 people are killed each year when a vehicle experiences rollover [**4**]. For this reason, the safety focus in industry and government has increasingly looked at rollover prevention.

For example, the National Highway Traffic Safety Administration (NHTSA) has recently begun roll stability evaluation of vehicles using their New Car Assessment Program (NCAP). The review consists of calculating a Static Stability Factor (SSF), which is based on the height of the center of gravity of the vehicle and its track width, and a dynamic maneuvering test [**4**]. The SSF is given a larger weighting in the rating, however, and the dynamic test is limited. This is not necessarily a good measure of rollover stability since the SSF is based on only static measurements for steady-state maneuvers [**5**]. In a real rollover situation, driver input is a large factor in determining whether an accident will happen. The NHTSA admits that a vehicle with its highest rating of five stars still has a 10% chance of rollover in a single-vehicle accident. In fact, the number of rollover accidents for some five-star vehicles is higher than those of some three-star vehicles due to the increased likelihood of aggressive maneuvers in certain types of automobiles such as sports cars [**4**]. Furthermore, the ratings are primarily focused on tripped rollover, so they are not entirely relevant to the study of preventing un-tripped rollover.

Industry has also begun deploying many basic rollover prevention systems. One concept is the use of a variable ride-height suspension (VRHS) technique. Vehicles with high suspensions required for off-road travel can lower their suspension height for on-road, higher speed conditions and therefore decrease the probability of rollover [**6**]. Active suspensions are also a common feature. Anti-roll bars are used to help reduce the roll angle of vehicles [**7**]. Other methods include traction and electronic stability controls (ESC) [**8**]. The feasibility of active torsion bar control systems is also a current research topic [**9**]. Algorithms are also being developed by manufacturers to prevent rollover, but the details often are not shared with the public for proprietary reasons.

The development of rollover prevention systems is promising. For example, ESC reduces the odds of fatal rollovers by 73 percent in SUVs and 40 percent in passenger cars, according to the University of Michigan Transportation Research Institute [**10**]. Ford plans to include rollover-reducing ESC as a standard feature in all vehicles by 2009

[**11**]. The technology is actually going to be federally required for all vehicles in the future [**10**].

Changing the dynamics of the vehicle is not the only way to prevent rollover. Research is also leading to methods that involve predicting when wheel lift will occur so that a driver can be warned of the danger. Time-To-Rollover (TTR) metrics, which are used to find the amount of time it takes for rollover to occur after a given steering input, are also being used in research [**12**]. The amount of time, however, is too small for a human to react in time [**5**]. If this method is implemented, it will be necessary to use a system to make the necessary changes in steering for a safe maneuver.

1.1.2 Study of Rollover Dynamics and Conditions

The dynamics of vehicle rollover are difficult to model. There are many parameters such as roll stiffness and damping that are challenging to measure. The limited amount of funds available in the academic realm for purchasing vehicles to collect data also makes research difficult. Multiple vehicle roll models have been developed by researchers in the field including those by Carlson and Gerdes, Mammar, and Kim and Park [**13-15**]. In previous work by the research group, many of these models were studied and narrowed down to a few that were validated experimentally by the authors and used model parameters that can be measured or inferred [**16**].

It is also important to understand the human factors that lead to rollover. It is challenging to foresee the steering input of a human driver in an emergency maneuver. Attempts to model drivers have been made, but none of them accurately model every single possible scenario [**5**]. When predicting rollover, various steering inputs must be considered and their effects must be studied.

Research in steering modification has also been initiated. One of the most obvious ways to prevent rollover is to never allow an unsafe steering input. This can be achieved by using a steer-by-wire system. Such systems used to help control yaw rate have been designed since the 1980s [**17**]. These controllers are now being developed to maintain roll stability [**13**]. Both feed-forward and feedback controllers were studied in previous work by the research group [**5**]. Further testing and experimental validation of these control methods may lead to working control systems that will successfully mitigate unsafe steering inputs. Before developing these algorithms, an understanding of the effects of the steering input must be achieved.

1.1.3 Scaled Vehicle Testing

Testing roll models and algorithms created to prevent rollover can become extremely complicated and expensive. If scaled vehicles could be used instead, the costs can be reduced and safety concerns can be eliminated. The dynamics of a scaled vehicle have been shown to be similar enough to those of actual vehicles through dimensional analysis to be used for testing controllers [**18**]. The vehicles can also easily be tested at various road conditions, including a banked surface, that are likely to promote rollover.

1.2 Outline of Remaining Chapters

The remainder of this thesis will be organized as follows: First, a two-degree-of-freedom model will be derived and the threshold for tire saturation will be explored in Chapter 2. Then, a three-degree-of-freedom model will be derived to incorporate roll dynamics in Chapter 3. The threshold for wheel lift will be calculated and compared to the threshold for tire saturation to predict whether a vehicle will first experience slip or roll.

Chapter 4 will present a feedforward control method to prevent wheel lift by modifying the steering input and reducing the restoring moment acting on the vehicle's suspension. Chapter 5 will explore how a banked road surface will affect the likelihood of rollover and demonstrate how a similar control algorithm can be used to prevent wheel lift in this situation. The algorithm will be tested through experiment using a scaled vehicle in Chapter 6. The main conclusions of the work will be discussed in Chapter 7.

1 J. Porretto, "Your car could be your wingman/ Automakers testing smart safety devices," *Houston Chronicle*, pp.1, 2003.

2 Anonymous, "Safety in the Driver's Seat," *Newsweek*, 145(21), pp. A6, 2005.

3. J. O'Donnell, "New cars help drivers avoid crashes; Radar scans hazards; system warns when car drifts out of lane," *USA Today*, pp. B3, 2005.

4. "Rollover," *SaferCar.gov*, National Highway Traffic Safety Administration, *http://www.safercar.gov/Rollover/Index.htm*.

5. J.T. Cameron, "Vehicle Dynamic Modeling for the Prediction and Prevention of Vehicle Rollover," M.S. Thesis, Mechanical and Nuclear Engineering, Pennsylvania State University, Dec. 2005.

6. “Variable Ride-Height Suspension (VRHS),” *Accident Reconstruction Newsletter*, 6(8),2004, *http://www.accidentreconstruction.com/newsletter/aug04/vrhs.asp.*

7. A. Lee, "Coordinated Control of Steering and Anti-Roll Bars to Alter Vehicle Rollover Tendencies." Journal of Dynamic Systems, Measurement, and Control, 124, pp. 127, 2002.

8. D. Konik, R. Bartz, F. Barnthol, H. Bruns, and M. Wimmer, "Dynamic Drive: System Description and Functional Improvements," presented at Proceedings of the 5th International Symposium on Advanced Vehicle Control (AVEC), Ann Arbor, Michigan, 2000.

9. D. Cimba, J. Wagner, A. Baviskar, “Investigation of Active Torsion Bar Actuator Configurations to Reduce Vehicle Body Roll,” *Vehicle System Dynamics*, 44(9), pp. 719-736, 2006.

10. D. Shepardson, “New Rules for Greater Auto Safety/ Feds to require systems to boost control, prevent rollovers,” *Houston Chronicle*, pp.1., 2006.

11. “Ford Speeds Up Making Rollover Stabilizers Standard,” *Financial Wire*, pp. 1, 2006.

12. B.-C. Chen and H. Peng, "A Real-time Rollover Threat Index for Sports Utility Vehicles," presented at Proceedings of the 1999 American Control Conference, San Diego, California, 1999.

13. C. Carlson and C. Gerdes, "Optimal Rollover Prevention with Steer by Wire and Differential Braking." Proceedings of IMECE ASME International Mechanical Engineering Congress, Washington, D.C., 2003.

14. S. Mammar, “Speed Scheduled Vehicle Lateral Control,” presented at Proceedings of the 1999 IEEE/IEEJ/JSAI International Conference on Intelligent Transportation Systems, 1999.

15. H.-J. Kim and Y.-P. Park, “Investigation of robust roll motion control considering varying speed and actuator dynamics,” *Mechatronics*, 2003.

16. J. Cameron and S. Brennan, “A Comparative, Experimental Study of Model Suitability to Describe Vehicle Rollover Dynamics for Controller Design,” Proceedings of the 2005 ASME IMECE, Dynamic Systems and Control Division, pp. 405-414, 2005.

17. S. Kueperkoch, J. Ahmed, A. Kojic, and J.-P. Hathout, "Novel Vehicle Stability Control Using Steer-by-Wire and Independent Four Wheel Torque Distribution." Washington, D.C, pp. 413-420, 2003.

18. S. Brennan and A. Alleyne, "Using a Scale Testbed: Controller Design and Evaluation." *IEEE Control Systems Magazine*, 21(3), pp. 15-26, 2001.

Chapter 2

Two-Degree-of-Freedom-Model

The chassis dynamics of vehicles are often described using a simplified Two-Degree-of-Freedom (2DOF) model, and so it is important to understand this basic model before studying the Three-Degree-of-Freedom (3DOF) models which incorporate roll dynamics. This chapter will present the 2DOF model by describing the assumptions associated with the model, the corresponding force equations resulting from Newtonian mechanics, and the final equations of motion. The equations of motion will then be used to find both the algebraic forms of the transfer functions and state space models for various inputs such as steering angle and outputs such as lateral velocity, yaw rate, and tire slip.

2.1 The Bicycle Model

The classical "bicycle model," which only describes lateral and yaw dynamics, will be used for the 2DOF analysis of this chapter. To derive this model, the Society of Automotive Engineers (SAE) body-fixed coordinate system will be used [**1**]. This coordinate system is shown in Figure **2-1**, and the parameters for this model are defined in Table **2-1**. The lateral velocity and yaw rate are often chosen as the state space variables. To better demonstrate these parameters, the slip coordinate model is shown in Figure **2-2**

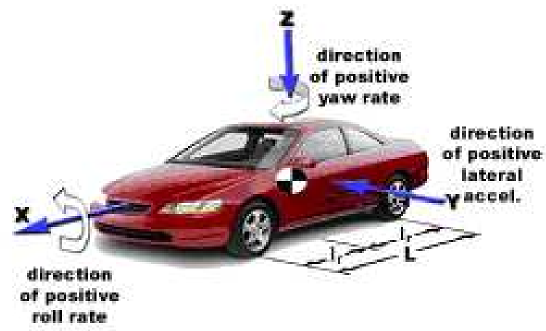

Figure **2-1**: SAE Vehicle Coordinate System

Table **2-1**: Parameters for 2DOF Model

Parameter	Definition
U	Longitudinal Velocity (body-fixed frame)
r	Yaw rate (angular rate about vertical axis)
m	Vehicle mass
I_{zz}	Inertia about the vehicle axis
l_f	Front-axle-to-CG distance
l_r	Rear-axle-to-CG distance
L	Track of vehicle ($l_f + l_r$)
t	Width of vehicle
β	Slip angle of the vehicle body
C_f	Front cornering stiffness
C_r	Rear cornering stiffness
δ_f	Front steering angle
α	Tire side-slip angle

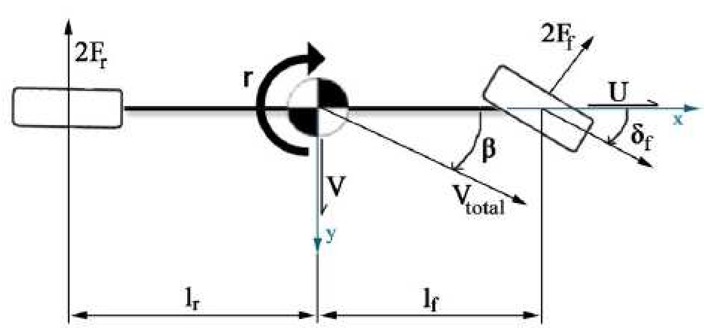

Figure **2-2**: Slip Coordinate Model

Certain assumptions are necessary to derive the equations of motion for the bicycle model. First, small angles are assumed such that $\cos(\theta) \approx 1$ and $\sin(\theta) \approx \theta$. The longitudinal velocity, U, is assumed to be constant. It is also assumed that the lateral force acting on a tire is linearly proportional to its side-slip angle. The tire side-slip angle, α, is defined as the difference between the longitudinal axis of the tire and the tire's local velocity vector, V_{tire}, and can be clearly seen in Figure **2-3**. Another assumption is that the tires must be rolling without slipping in the longitudinal direction. Finally, the forces acting on the right half of the vehicle are assumed to be symmetric to the forces acting on the left half of the vehicle. The last assumption simplifies the four-tire model to the single-track model with only two tires that looks similar to a bicycle, hence the name "bicycle model." However, the dynamics of an actual bicycle are notably different from this representation such that, ironically, the bicycle model is not suitable to describe the motion of a bicycle.

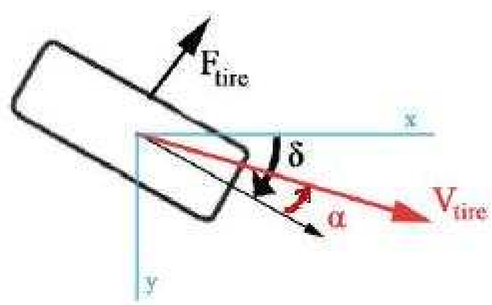

Figure **2-3**: Tire Velocity Vectors

2.1.1 Newtonian Force Equations for the 2DOF Model

Now that the parameters and assumptions have been defined, the force equations can be derived. As mentioned before, the side-slip angle of a tire is defined as the difference between the steering angle of the tire and the tire's local velocity vector, V_{tire}, as shown in Figure **2-3**. The lateral force on the tire is related to the side-slip angle by a constant called the cornering stiffness. The front and rear tires have different values for the cornering stiffness and are defined as C_f and C_r respectively. The units for these terms are *N/rad*. This relationship is shown in Eq. **2.1**

$$\begin{aligned} F_f &= C_f \alpha_f \\ F_r &= C_r \alpha_r \end{aligned} \qquad \textbf{2.1}$$

and again in matrix form in Eq. **2.2**

$$\begin{bmatrix} F_f \\ F_r \end{bmatrix} = \begin{bmatrix} C_f & 0 \\ 0 & C_r \end{bmatrix} \begin{bmatrix} \alpha_f \\ \alpha_r \end{bmatrix} \qquad \textbf{2.2}$$

By examining Figure **2-3**, the slip angles of each tire may be redefined as a ratio of the local velocities of each tire. The true velocity vector, V_{tire}, is offset from the longitudinal axis by the side-slip angle α. From geometry, the new relationship is found in Eq. **2.3**.

$$\alpha = \tan^{-1}\left(\frac{V_{tire,\,y}}{V_{tire,\,x}}\right) \approx \frac{V_{tire,\,y}}{V_{tire,\,x}} \qquad \textbf{2.3}$$

Now returning to Figure **2-2**, the lateral velocity vectors for the front and rear tire can be found.

$$\begin{aligned} V_{tire,y,front} &= V + l_f r \\ V_{tire,y,rear} &= V - l_r r \end{aligned} \qquad \textbf{2.4}$$

These definitions can be substituted into Eq. **2.3** to give the slip angles for the front and rear tires shown in Eq. **2.5** and Eq. **2.6**.

$$\alpha_f = \left(\frac{V + l_f r}{U}\right) - \delta_f \qquad \textbf{2.5}$$

$$\alpha_r = \left(\frac{V - l_r r}{U}\right) - \delta_r \qquad \textbf{2.6}$$

Assuming there is no rear steering input results in the final equations for the front and rear tire slip angles in matrix form:

$$\begin{bmatrix} \alpha_f \\ \alpha_r \end{bmatrix} = \begin{bmatrix} \frac{1}{U} & \frac{l_f}{U} \\ \frac{1}{U} & -\frac{l_r}{U} \end{bmatrix} \begin{bmatrix} V \\ r \end{bmatrix} + \begin{bmatrix} -1 \\ 0 \end{bmatrix} \delta_f \qquad \textbf{2.7}$$

Now the Newtonian force equations can be found by substituting the tire slip equations into Eq. **2.1**.resulting in the following algebraic force equations which are written in matrix form in Eq. **2.10**

$$F_f = C_f \alpha_f = C_f \left(\frac{V + l_f r}{U} - \delta_f\right) \qquad \textbf{2.8}$$

$$F_r = C_r \alpha_r = C_r \left(\frac{V - l_r r}{U}\right) \qquad \textbf{2.9}$$

$$\begin{bmatrix} F_f \\ F_r \end{bmatrix} = \begin{bmatrix} C_f \alpha_f \\ C_r \alpha_r \end{bmatrix} = \begin{bmatrix} \frac{C_f}{U} & \frac{C_f l_f}{U} \\ \frac{C_r}{U} & -\frac{C_r l_r}{U} \end{bmatrix} \begin{bmatrix} V \\ r \end{bmatrix} + \begin{bmatrix} -C_f \\ 0 \end{bmatrix} \delta_f \qquad \textbf{2.10}$$

2.1.2 Motion Equations for the 2DOF Model

Now the equations of motion for the bicycle model can be developed. The system described above, however, is a non-Newtonian system because the lateral velocity and yaw rate are given in body-fixed coordinates. Since the bicycle model was formulated with respect to the vehicle frame, the equations of motion for the vehicle with respect to Earth-fixed axes must be developed. First, the longitudinal and lateral accelerations must be found. If $\vec{\omega}$ is the angular velocity of the body-fixed axes (x,y,z), and $\vec{P}$ is a vector whose components are time-varying with respect to the same axes, the time derivative of the vector can be calculated [**2**].

$$\dot{\vec{P}} = \frac{d\vec{P}}{dt} + \vec{\omega} \times \vec{P} \qquad \textbf{2.11}$$

Therefore, the accelerations relative to the body-fixed axes may be expressed by taking the derivative of the velocity vector $\vec{v}$ as in Eq. **2.12**.

$$\vec{a} = \vec{\omega} \times \vec{v} + \dot{\vec{v}} \qquad \textbf{2.12}$$

Here, $\vec{a}$ is the total acceleration of the body in global coordinates, $\dot{\vec{v}}$ is the time rate of change of $\vec{v}$ in global coordinates, and $\vec{\omega}$ is the vehicle's yaw rate in body-fixed coordinates.

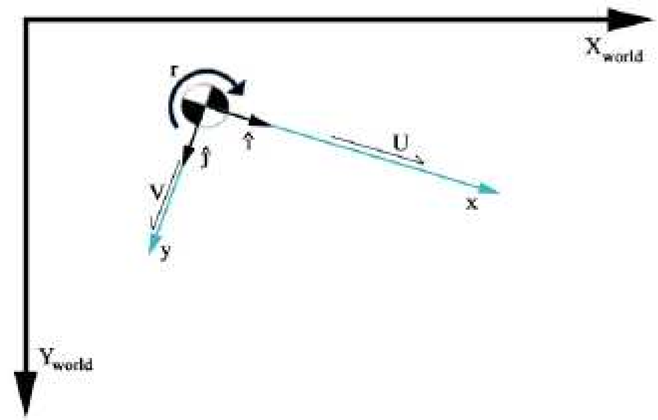

Figure **2-4**: Motion of a Body-Fixed Coordinate System

The velocities U and V have already been defined to be along the x- and y- axes of the body-fixed frame respectively as shown in Figure **2-4** . If the unit vectors of the body-fixed (x,y,z) coordinate system are ($\hat{\imath}, \hat{\jmath}, \hat{k}$) and

$$\vec{\omega} = r \cdot \hat{k} \qquad \textbf{2.13}$$

Eq. **2.12** can be expressed as:

$$\vec{a} = \left(r\hat{k} \times U\hat{\imath}\right) + \left(r\hat{k} \times V\hat{\jmath}\right) + \dot{U}\hat{\imath} + \dot{V}\hat{\jmath} \qquad \textbf{2.14}$$

which becomes:

$$\vec{a} = -r \cdot V\hat{\imath} + \dot{U}\hat{\imath} + r \cdot U\hat{\jmath} + \dot{V}\hat{\jmath} \qquad \textbf{2.15}$$

after taking the vector cross product. The terms can be separated to give the x and y components of acceleration:

$$a_x = \dot{U} - Vr \qquad \textbf{2.16}$$

$$a_y = \dot{V} + Ur \qquad \textbf{2.17}$$

Eq. **2.16** is equal to zero due to the previous assumption that longitudinal velocity is constant and the tires are rolling without slipping. Therefore the acceleration along the longitudinal axis is zero. This means there are no net forces acting along the x-axis. By summing the forces in the lateral direction and the moments about the vertical axis, the equations of motion are formed.

$$\begin{aligned} \sum F_y &= m(\dot{V} + Ur) = F_f + F_r \\ \sum M_z &= I_{zz}\dot{r} = F_f l_f - F_r l_r \end{aligned} \qquad \textbf{2.18}$$

Substituting Eq. **2.8** and Eq. **2.9** into the equations of motion results in:

$$\begin{aligned} m\left(\dot{V} + rU\right) &= C_f \frac{(V + l_f r)}{U} + C_r \frac{(V - l_r r)}{U} - C_f \delta_f \\ I_{zz}\dot{r} &= C_f \frac{(V + l_f r)}{U} l_f - C_f l_f \delta_f - C_r \frac{(V - l_r r)}{U} l_r \end{aligned} \qquad \textbf{2.19}$$

Rearranging the equations gives:

$$\begin{aligned} \dot{V} &= \frac{C_f + C_r}{mU} V + \left(\frac{C_f l_f - C_r l_r}{mU} - U \right) r - \frac{C_f}{m} \delta_f \\ \dot{r} &= \frac{C_f l_f - C_r l_r}{I_{zz} U} V + \frac{C_f l_f^{\,2} + C_r l_r^{\,2}}{I_{zz} U} r - \frac{C_f l_f}{I_{zz}} \delta_f \end{aligned} \qquad \textbf{2.20}$$

Recognizing the state space matrices terms of the dynamic matrix A and the input matrix B:

$$
\begin{aligned}
a_{11} &= \frac{C_f + C_r}{mU} \\
a_{12} &= \frac{C_f l_f - C_r l_r}{mU} - U \\
a_{21} &= \frac{C_f l_f - C_r l_r}{I_{zz} U} \\
a_{22} &= \frac{C_f l_f^{\,2} + C_r l_r^{\,2}}{I_{zz} U} \\
b_1 &= -\frac{C_f}{m} \\
b_2 &= -\frac{C_f l_f}{I_{zz}}
\end{aligned} \tag{2.21}
$$

$$
\begin{aligned}
\dot{V} &= a_{11} V + a_{12} r + b_1 \delta_f \\
\dot{r} &= a_{21} V + a_{22} r + b_2 \delta_f
\end{aligned} \tag{2.22}
$$

the equations of motion can be written in the state space model form:

$$
\begin{bmatrix} \dot{V} \\ \dot{r} \end{bmatrix} = \begin{bmatrix} a_{11} & a_{12} \\ a_{21} & a_{22} \end{bmatrix} \begin{bmatrix} V \\ r \end{bmatrix} + \begin{bmatrix} b_1 \\ b_2 \end{bmatrix} \delta_f \tag{2.23}
$$

or with the substituted coefficients:

$$
\begin{bmatrix} \dot{V} \\ \dot{r} \end{bmatrix} = \begin{bmatrix} \dfrac{C_f + C_r}{mU} & \dfrac{C_f l_f - C_r l_r}{mU} - U \\ \dfrac{C_f l_f - C_r l_r}{I_{zz} U} & \dfrac{C_f l_f^{\,2} + C_r l_r^{\,2}}{I_{zz} U} \end{bmatrix} \begin{bmatrix} V \\ r \end{bmatrix} + \begin{bmatrix} -\dfrac{C_f}{m} \\ -\dfrac{C_f l_f}{I_{zz}} \end{bmatrix} \delta_f \tag{2.24}
$$

The algebraic transfer functions can also be derived from Eq. **2.22**.

$$
\begin{aligned}
sV(s) &= a_{11} V(s) + a_{12} r(s) + b_1 \delta_f(s) \\
sr(s) &= a_{21} V(s) + a_{22} r(s) + b_2 \delta_f(s)
\end{aligned} \tag{2.25}
$$

Then they can easily be solved for V(s) and r(s) as shown in Eq. **2.26**.

$$r(s) = \frac{(s - a_{11})V(s) - b_1\delta_f(s)}{a_{12}}$$
$$V(s) = \frac{(s - a_{22})r(s) - b_2\delta_f(s)}{a_{21}} \qquad \textbf{2.26}$$

Then these two equations can be substituted into each other:

$$r(s) = \frac{(s - a_{11})\left(\frac{(s - a_{22})r(s) - b_2\delta_f(s)}{a_{21}}\right) - b_1\delta_f(s)}{a_{12}}$$
$$V(s) = \frac{(s - a_{22})\left(\frac{(s - a_{11})V(s) - b_1\delta_f(s)}{a_{12}}\right) - b_2\delta_f(s)}{a_{21}} \qquad \textbf{2.27}$$

Solving Eq. **2.27** for the output to input ratio results in:

$$\frac{r(s)}{\delta_f(s)} = \frac{\frac{(s - a_{11})b_2}{a_{21}} + b_1}{\frac{(s - a_{11})(s - a_{22})}{a_{21}} - a_{12}}$$
$$\frac{V(s)}{\delta_f(s)} = \frac{\frac{(s - a_{22})b_1}{a_{12}} + b_2}{\frac{(s - a_{11})(s - a_{22})}{a_{12}} - a_{21}} \qquad \textbf{2.28}$$

And finally, after some distributing and rearranging, the transfer functions are:

$$\frac{r(s)}{\delta_f(s)} = \frac{b_2 s + (b_1 a_{21} - a_{11} b_2)}{s^2 - (a_{11} + a_{22})s + (a_{11}a_{22} - a_{12}a_{21})}$$
$$\frac{r(s)}{\delta_f(s)} = \frac{b_2 s + (b_1 a_{21} - a_{11} b_2)}{s^2 - (a_{11} + a_{22})s + (a_{11}a_{22} - a_{12}a_{21})} \qquad \textbf{2.29}$$

To caution there were no mistakes, in either the state-space or transfer-function formulations, the models were compared. Both the state space method and the transfer function method resulted in the same Bode plots for lateral velocity and yaw rate which can be seen for various longitudinal velocities for a given vehicle in Figure **2-5**.

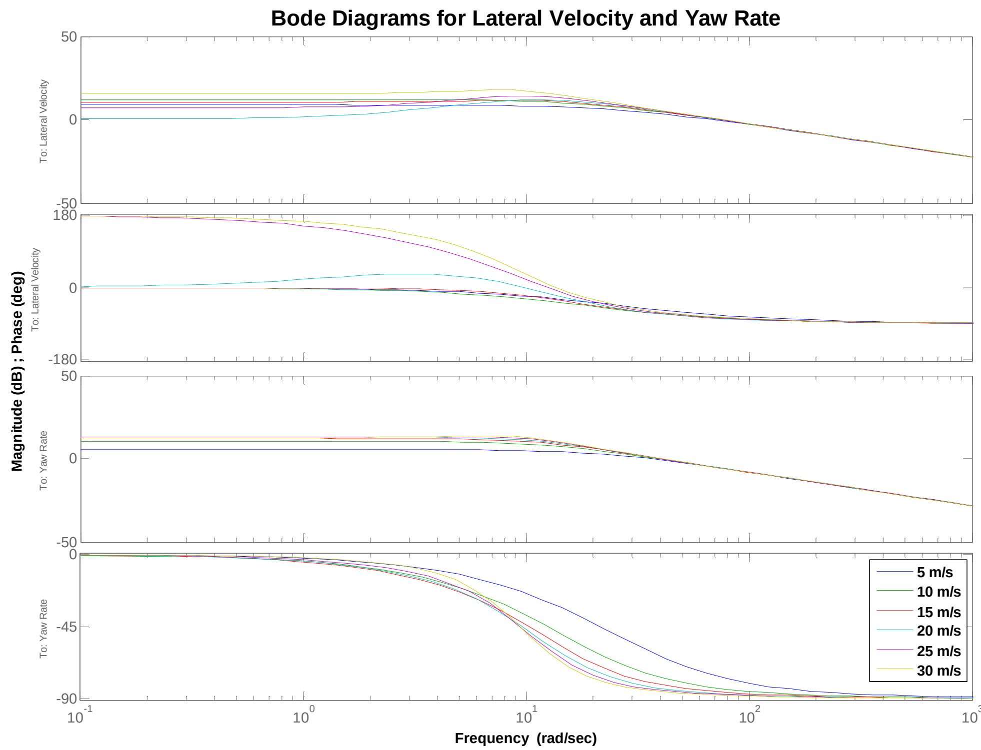

Figure **2-5**: Bode Diagrams for the Transfer Functions for Front Steering Input to Lateral Velocity and Yaw Rate Output for the Bicycle Model

The next point of interest is the set of equations describing tire slip due to steering input. Returning to the state space model in Eq. **2.23** and Eq. **2.24** , the state variables were chosen as the lateral velocity V and the yaw rate r. These were also chosen as the output variables, so the output matrix C and the direct transmission matrix D were self-evident for the state space model. To modify the model such that tire slip will be the output, the C and D matrices must be chosen accordingly. Returning to Eq. **2.7** for tire slip in terms of V and r, the state space matrices terms can be recognized as those shown in Eq. **2.30**

$$\begin{aligned} c_{11} &= \frac{1}{U} \\ c_{12} &= \frac{l_f}{U} \\ c_{21} &= \frac{1}{U} \\ c_{22} &= -\frac{l_r}{U} \\ d_1 &= -1 \\ d_2 &= 0 \end{aligned} \qquad \textbf{2.30}$$

The second state space equation can be written as:

$$\begin{bmatrix} \alpha_f \\ \alpha_r \end{bmatrix} = \begin{bmatrix} c_{11} & c_{12} \\ c_{21} & c_{22} \end{bmatrix} \begin{bmatrix} V \\ r \end{bmatrix} + \begin{bmatrix} d_1 \\ d_2 \end{bmatrix} \delta_f \qquad \textbf{2.31}$$

The generic transfer function for input u(t) and output y(t) can be written in terms of the four state space matrices:

$$\frac{Y(s)}{U(s)} = C \cdot (sI - A)^{-1} \cdot B + D \qquad \textbf{2.32}$$

For front and rear slip, the transfer functions can be written in matrix or algebraic form:

$$\begin{aligned} \frac{\alpha_f(s)}{\delta_f(s)} &= \begin{bmatrix} c_{11} & c_{12} \end{bmatrix} \left[\begin{bmatrix} s & 0 \\ 0 & s \end{bmatrix} - \begin{bmatrix} a_{11} & a_{12} \\ a_{21} & a_{22} \end{bmatrix} \right]^{-1} \begin{bmatrix} b_1 \\ b_2 \end{bmatrix} + d_1 \\ \frac{\alpha_r(s)}{\delta_f(s)} &= \begin{bmatrix} c_{21} & c_{22} \end{bmatrix} \left[\begin{bmatrix} s & 0 \\ 0 & s \end{bmatrix} - \begin{bmatrix} a_{11} & a_{12} \\ a_{21} & a_{22} \end{bmatrix} \right]^{-1} \begin{bmatrix} b_1 \\ b_2 \end{bmatrix} + d_2 \end{aligned} \qquad \textbf{2.33}$$

$$\begin{aligned} \frac{\alpha_f(s)}{\delta_f(s)} &= \frac{d_1 s^2 + (c_{11}b_1 + c_{12}b_2 - d_1(a_{11} + a_{22}))s + (c_{11}(b_2 a_{12} - b_1 a_{22}) + c_{12}(b_1 a_{21} - b_2 a_{11}) + d_1(a_{11}a_{22} - a_{12}a_{21}))}{s^2 - (a_{11} + a_{22})s + (a_{11}a_{22} - a_{12}a_{21})} \\ \frac{\alpha_r(s)}{\delta_f(s)} &= \frac{d_2 s^2 + (c_{21}b_1 + c_{22}b_2 - d_2(a_{11} + a_{22}))s + (c_{21}(b_2 a_{12} - b_1 a_{22}) + c_{22}(b_1 a_{21} - b_2 a_{11}) + d_2(a_{11}a_{22} - a_{12}a_{21}))}{s^2 - (a_{11} + a_{22})s + (a_{11}a_{22} - a_{12}a_{21})} \end{aligned} \qquad \textbf{2.34}$$

Again, both the state space method and the transfer function method result in the same Bode plots for front and rear tire slip which can be seen for various longitudinal velocities for a given vehicle in Figure **2-6** and Figure **2-7**.

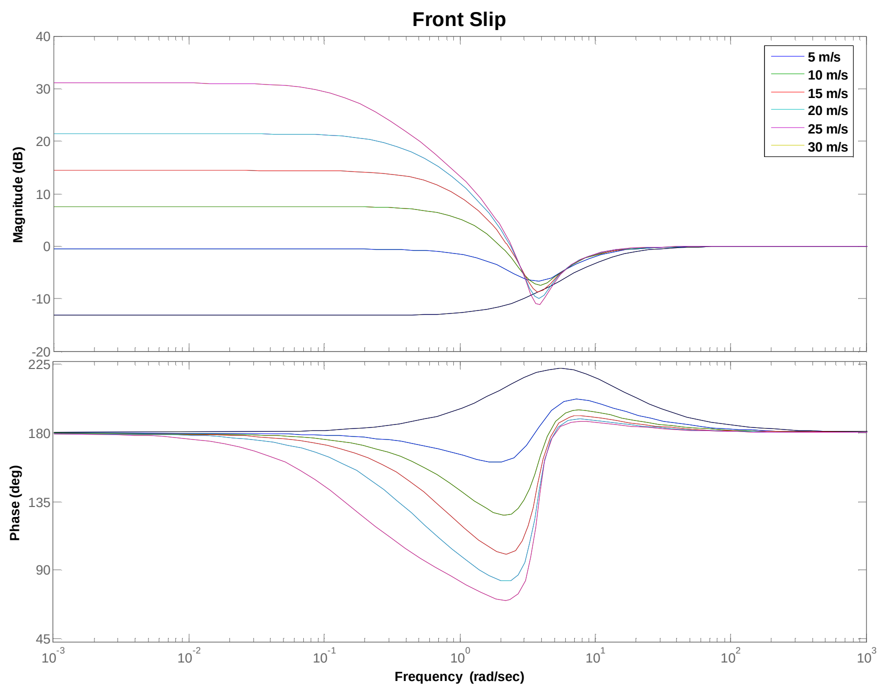

Figure **2-6**: Bode Diagram for the Transfer Function for Front Steering Input to Front Tire Slip Angle Output for the Bicycle Model

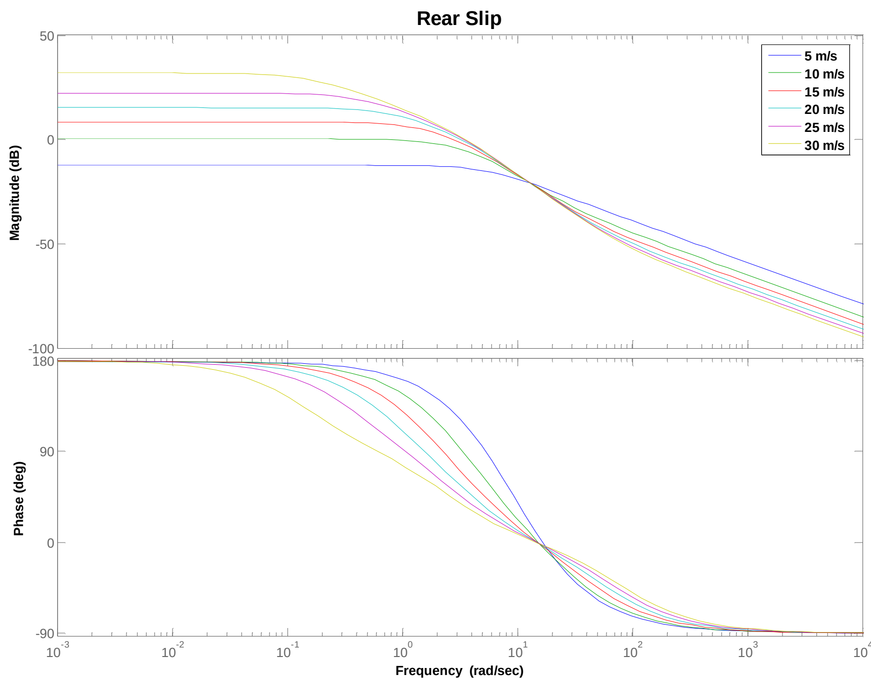

Figure **2-7**: Bode Diagram for the Transfer Function for Front Steering Input to Rear Tire Slip Angle Output for the Bicycle Model

Using the ratio of slip angle to steering input, the maximum steering input before tire saturation and slip occurs can be calculated by substitution of a known maximum slip angle. The ratio of slip angle to steering input is found from the Bode analysis done previously. Because tires cannot produce an unlimited amount of force, the tires will begin to skid at some maximum slip angle, which through experiment is found to be approximately 10 degrees [**3**]. Assuming that tire saturation occurs when the slip angle is at this maximum value, the following equation can be used to find the steering angle at which saturation occurs by substituting the 10 degree value in for $\alpha_{f\max}$.

$$\delta_{f,\max} = \left(\frac{\alpha}{\delta_f} \right)^{-1} \alpha_{f\max} \qquad \textbf{2.35}$$

This maximum steering input can then be plotted against the frequency to see which steering frequencies are most likely to cause slip as seen in Figure **2-8** and Figure **2-9**.

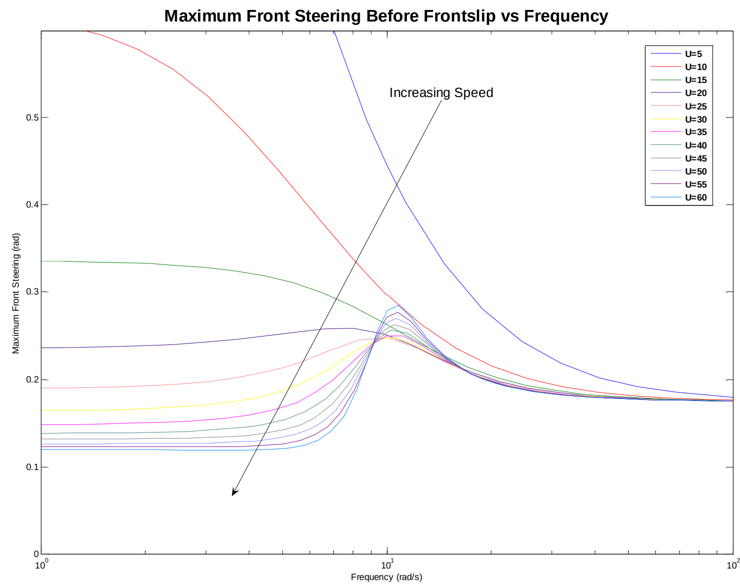

Figure **2-8**: Front Steering Input that Causes Front Tire Saturation for the Bicycle Model

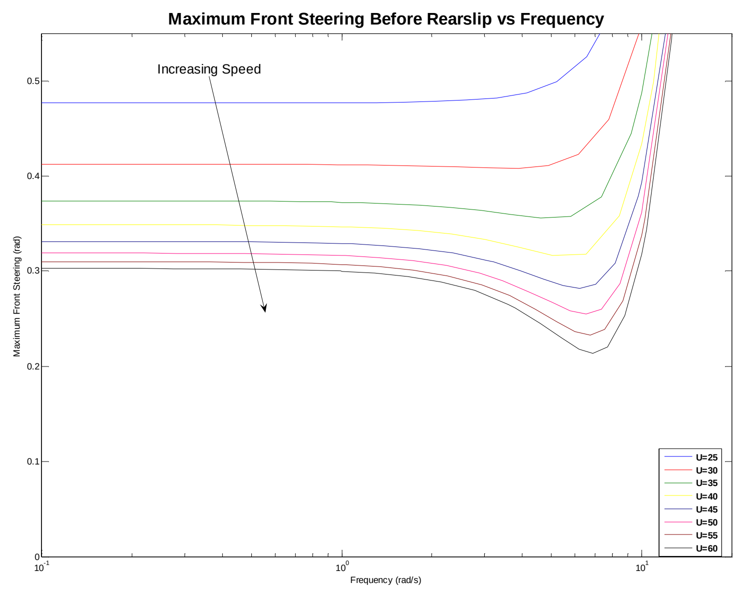

Figure **2-9**: Front Steering Input that Causes Rear Tire Saturation for the Bicycle Model

2.2 Conclusions

In this chapter, the simple bicycle model was derived using Newtonian mechanics. Then these equations were manipulated into the state space form to see how a front steering input affects lateral velocity, yaw rate, and tire slip. These results will be compared to those of a more complicated model in later chapters to verify their accuracy. Methods similar to the ones used to find steering inputs which cause tire slip will be used to find the inputs at the threshold for wheel lift, and hence roll. The two cases will be compared to determine whether slip or roll occurs first at various steering inputs.

1. "Surface Vehicle Recommended Practice," Society of Automotive Engineers J670e, July 1976.

2. J.H. Ginsberg, *Advanced Engineering Dynamics*, 2nd ed. New York, NY: Cambridge University Press, 1998.

3. J.C. Dixon, *Tires, Suspension, and Handling*, 2nd Ed. Warrendale, PA: The Society of Automotive Engineers (SAE), 1996.

Chapter 3

Three-Degree-of-Freedom Model

Although the bicycle model is helpful in describing simple vehicle dynamics, a Three-Degree-of-Freedom (3DOF) model must be used if one wishes to consider roll dynamics. This chapter will present a 3DOF model including its derivation and its state space representation. In previous work by the research group and in literature, multiple roll models have been developed for study [**1**]. This chapter, for brevity, focuses on one model in particular. Using this model, the conditions for wheel lift will be explored. The steering inputs necessary for wheel lift are then compared to those necessary for tire slip to find which will occur first at various steering conditions.

3.1 Roll Model

The roll model chosen for examination in this work was originally created and published by Kim and Park [**2**]. To include roll dynamics, this linear model incorporates roll angle degrees of freedom in addition to the lateral velocity and yaw rate motions described earlier. The same SAE coordinate system defined in the previous chapter will be used as shown in Figure **3-1**. The parameters for this model are defined in Table **3-1**. The roll angle is defined in Figure **3-2**.

The assumptions included in this model are similar to those of the bicycle model. First, small angles are assumed such that cos(θ) ≈ 1 and sin(θ) ≈ θ. The longitudinal velocity, U, is assumed to be constant. It is also assumed that the lateral force acting on a

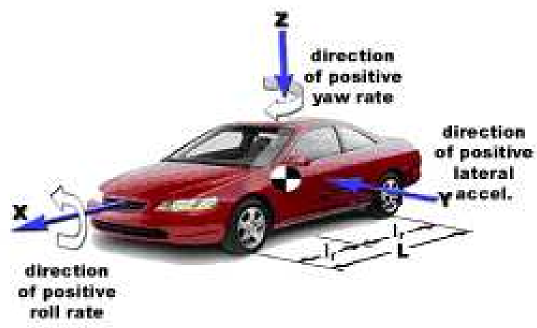

Figure **3-1**: SAE Vehicle Coordinate System

Table **3-1**: Parameters for 3DOF Model

Parameter	Definition
U	Longitudinal velocity (body-fixed frame)
r	Yaw rate (angular rate about vertical axis)
ϕ	Roll angle
$\dot{\phi}$	Roll rate
m	Vehicle mass
m_s	Sprung mass
m_u	Unsprung mass
I_{zz}	Inertia about the vehicle axis
I_{yy}	Inertia about the pitch axis
I_{xx}	Inertia about the roll axis
I_{xz}	Inertia product
l_f	Front-axle-to-CG distance
l_r	Rear-axle-to-CG distance
L	Track of vehicle ($l_f + l_r$)
t	Width of vehicle
h	Height of CG above roll axis
β	Slip angle of the vehicle body
C_f	Front cornering stiffness
C_r	Rear cornering stiffness
K_φ	Roll stiffness
D_φ	Roll damping
δ_f	Front steering angle
α	Tire side-slip angle

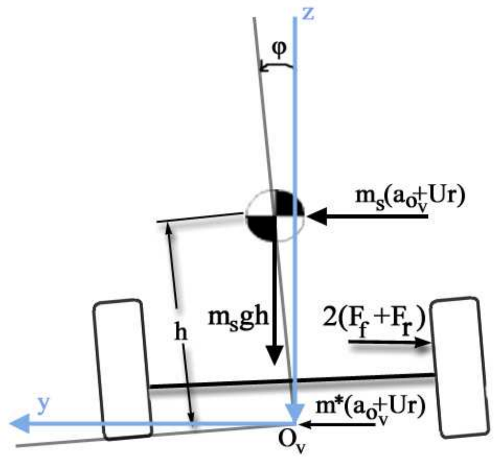

Figure **3-2**: Roll Angle Definition for 3DOF Model

tire is linearly proportional to its side-slip angle. Another assumption is that the tires must be rolling without slipping in the longitudinal direction. A new assumption is that the vehicle also has a sprung mass. The sprung mass is defined as all of the mass that is supported by the suspension [**3**]. For simplification, symmetry about the x-z plane will be assumed so that $I_{xz} = 0$.

3.1.1 Motion Equations

The motion equations may be developed using the kinematics methods described in [**4**]. The vehicle is subject to inertial forces and is affected by the motion of the center of gravity (CG) about the origin O_v. The coordinate system is not centered at the CG, so the equations of motion are expressed in terms of the acceleration at the origin a_{Ov} and the angular momentum about the origin H_{Ov}. Therefore the sum of the moments is expressed as:

$$\sum M_{Ov} = m_s \cdot h \times a_{Ov} + \dot{\vec{H}}_{Ov} \quad \textbf{3.1}$$

The angular momentum is defined as:

$$\vec{H}_{Ov} = [I] \cdot [\vec{\omega}] \quad \textbf{3.2}$$

where [I] is the inertia matrix:

$$[I] = \begin{bmatrix} I_{xx} & -I_{xy} & -I_{xz} \\ -I_{xy} & I_{yy} & -I_{yz} \\ -I_{xz} & -I_{yz} & I_{zz} \end{bmatrix} \quad \textbf{3.3}$$

and $[\vec{\omega}]$ is the angular velocity vector:

$$[\vec{\omega}] = \begin{bmatrix} \omega_x \\ \omega_y \\ \omega_z \end{bmatrix} \quad \textbf{3.4}$$

with components along the body-fixed axes. The inertial properties of the vehicle are constant since the vehicle is not moving with respect to the body-fixed axes. The time derivative of Eq. **3.2** is shown to be:

$$\dot{\vec{H}}_{Ov} = \frac{\partial \vec{H}_{Ov}}{\partial t} + [\vec{\omega}] \times \vec{H}_{Ov} = [I] \cdot [\vec{\alpha}] + \begin{bmatrix} 0 & -\omega_z & \omega_y \\ \omega_z & 0 & -\omega_x \\ -\omega_y & \omega_x & 0 \end{bmatrix} \cdot [I] \cdot [\vec{\omega}] \quad \textbf{3.5}$$

in [**4**] where α is the angular acceleration about the body-fixed coordinate axes.

Assuming that I_{xz}, I_{xy}, and I_{yz} are negligible, the inertia matrix can be simplified to:

$$[I] = \begin{bmatrix} I_{xx} & 0 & 0 \\ 0 & I_{yy} & 0 \\ 0 & 0 & I_{zz} \end{bmatrix} \quad \textbf{3.6}$$

From the geometry shown in Figure **3-2**, the angular velocity can be rewritten as:

$$[\vec{\omega}] = \begin{bmatrix} \omega_x \\ \omega_y \\ \omega_z \end{bmatrix} = \begin{bmatrix} \dot{\phi} \\ -r\sin(\phi) \\ -r\cos(\phi) \end{bmatrix} \qquad \textbf{3.7}$$

The angular acceleration can easily be found by taking the derivative of the angular velocity just found in Eq. **3.7**:

$$[\vec{\alpha}] = \begin{bmatrix} \alpha_x \\ \alpha_y \\ \alpha_z \end{bmatrix} = \begin{bmatrix} \ddot{\phi} \\ -\dot{r}\sin(\phi) - r\cos(\phi)\dot{\phi} \\ -\dot{r}\cos(\phi) + r\sin(\phi)\dot{\phi} \end{bmatrix} \qquad \textbf{3.8}$$

The angular acceleration is vital in calculating the change of angular momentum with respect to time. The linear acceleration is often broken down into two components [**4**]:

$$\vec{a}_{Ov} = \vec{a}_{Ov,n} + \vec{a}_{Ov,t} \qquad \textbf{3.9}$$

where the two terms are normal and tangential acceleration respectively. The two components may be defined as:

$$\vec{a}_{Ov,n} = [\vec{\omega}] \cdot U \qquad \textbf{3.10}$$

$$\vec{a}_{Ov,t} = [\vec{\alpha}] \cdot h \qquad \textbf{3.11}$$

Now returning to Eq. **3.1**, the total moment about the body-fixed axes can be found since the time rate of change of angular momentum and linear acceleration are known.

If the forces and moments are summed as they were in the previous chapter for the bicycle model, a set of non-linear equations results. Using the same lateral tire force equations as in the bicycle model and again assuming there are no longitudinal forces acting on the tires, the external forces acting on the vehicle can be found. In the roll model, a third equation for the moments about the x-axis is necessary:

$$\begin{bmatrix} m & 0 & m_s h \\ 0 & I_{zz} & 0 \\ m_s h & 0 & I_{xx} + m_s h^2 \end{bmatrix} \begin{bmatrix} \dot{V} \\ \dot{r} \\ \ddot{\phi} \end{bmatrix} + \begin{bmatrix} 0 & mU & 0 \\ 0 & 0 & 0 \\ 0 & m_s hU & D_\varphi \end{bmatrix} \begin{bmatrix} V \\ r \\ \dot{\phi} \end{bmatrix} + \begin{bmatrix} 0 & 0 & 0 \\ 0 & 0 & 0 \\ 0 & 0 & K_\varphi - m_s gh \end{bmatrix} = \begin{bmatrix} 1 & 1 \\ l_f & -l_r \\ 0 & 0 \end{bmatrix} \begin{bmatrix} F_f \\ F_r \end{bmatrix} \qquad \textbf{3.12}$$

The result in Eq. **3.12** is in the MDK form:

$$M \cdot \ddot{q} + D \cdot \dot{q} + K \cdot q = F \cdot u \qquad \textbf{3.13}$$

This form demonstrates the contributions from inertial, damping, and stiffness forces, but the equations would be easier to work with in the general state-space form with the state vector:

$$x = \lfloor V \quad r \quad \phi \quad \dot{\phi} \rfloor \qquad \textbf{3.14}$$

and input vector:

$$u = \lfloor F_f \quad F_r \rfloor \qquad \textbf{3.15}$$

in the form:

$$\frac{dx}{dt} = A \cdot x + B \cdot u \qquad \textbf{3.16}$$

This transformation can be completed by first defining the transformation matrices

$$R = \begin{bmatrix} 1 & 0 & 0 \\ 0 & 1 & 0 \\ 0 & 0 & 0 \\ 0 & 0 & 1 \end{bmatrix}, S = \begin{bmatrix} 0 & 0 & 0 \\ 0 & 0 & 0 \\ 0 & 0 & 1 \\ 0 & 0 & 0 \end{bmatrix}, T = \begin{bmatrix} 0 & 0 & 0 & 0 \\ 0 & 0 & 0 & 0 \\ 0 & 0 & 0 & 1 \\ 0 & 0 & 0 & 0 \end{bmatrix} \qquad \textbf{3.17}$$

$$E = R \cdot (M - I_3) \cdot R^T + I_4 \qquad \textbf{3.18}$$

where I_n represents the identity matrix of size n. The state space matrices are then defined as the following in terms of M, D, K, and F:

$$A = E^{-1} \cdot \left(- R \cdot D \cdot R^T - R \cdot K \cdot S^T + T\right)$$
$$B = E^{-1} \cdot \left(R \cdot F\right) \qquad \mathbf{3.19}$$

For direct comparison to the bicycle model, the model must be written in terms of steering input instead of the force input vector. As shown in the previous chapter, the lateral tire force is a function of the tire slip angle.

$$F = \begin{bmatrix} F_f \\ F_r \end{bmatrix} = \begin{bmatrix} C_f & 0 \\ 0 & C_r \end{bmatrix} \begin{bmatrix} \alpha_f \\ \alpha_r \end{bmatrix} = \overline{A}_F \overline{\alpha} \qquad \mathbf{3.20}$$

The tire slip angle can be written in terms of the lateral velocity, yaw rate, and front steering input.

$$\overline{\alpha} = \begin{bmatrix} \alpha_f \\ \alpha_r \end{bmatrix} = \begin{bmatrix} \frac{1}{U} & \frac{l_f}{U} \\ \frac{1}{U} & -\frac{l_r}{U} \end{bmatrix} \begin{bmatrix} V \\ r \end{bmatrix} + \begin{bmatrix} -1 \\ 0 \end{bmatrix} \delta_f \qquad \mathbf{3.21}$$

The slip angles can be expressed in terms of the new state vector using the same relationship:

$$\overline{\alpha} = \begin{bmatrix} \alpha_f \\ \alpha_r \end{bmatrix} = \begin{bmatrix} \frac{1}{U} & \frac{l_f}{U} & 0 & 0 \\ \frac{1}{U} & \frac{-b}{U} & 0 & 0 \end{bmatrix} \begin{bmatrix} V \\ r \\ \phi \\ \dot{\phi} \end{bmatrix} + \begin{bmatrix} -1 \\ 0 \end{bmatrix} \delta_f = \overline{A}_\alpha x + \overline{B}_\alpha \delta_f \qquad \mathbf{3.22}$$

Now returning to Eq. **3.16** where the force was used as the input, a new state-space model with steering as the input can be derived by substituting the relationships in Eq. **3.20** and Eq. **3.22**.

$$\frac{dx}{dt} = A \cdot x + B \cdot F$$
$$\frac{dx}{dt} = A \cdot x + B \cdot (\overline{A}_F \cdot \overline{\alpha})$$
$$\frac{dx}{dt} = A \cdot x + B \cdot \overline{A}_F \cdot \left[\left(\overline{A}_\alpha \cdot x\right) + \left(\overline{B}_\alpha \cdot \delta_f\right)\right] \tag{3.23}$$
$$\frac{dx}{dt} = \left(A + B \cdot \overline{A}_F \cdot \overline{A}_\alpha\right)x + \left(B \cdot \overline{A}_F \cdot \overline{B}_\alpha\right)\delta_f$$

The Bode plots for lateral velocity, yaw rate, roll angle, and roll rate can be plotted using the state-space model in Eq. **3.23**. The Bode plot for roll angle is shown in Figure **3-3**.

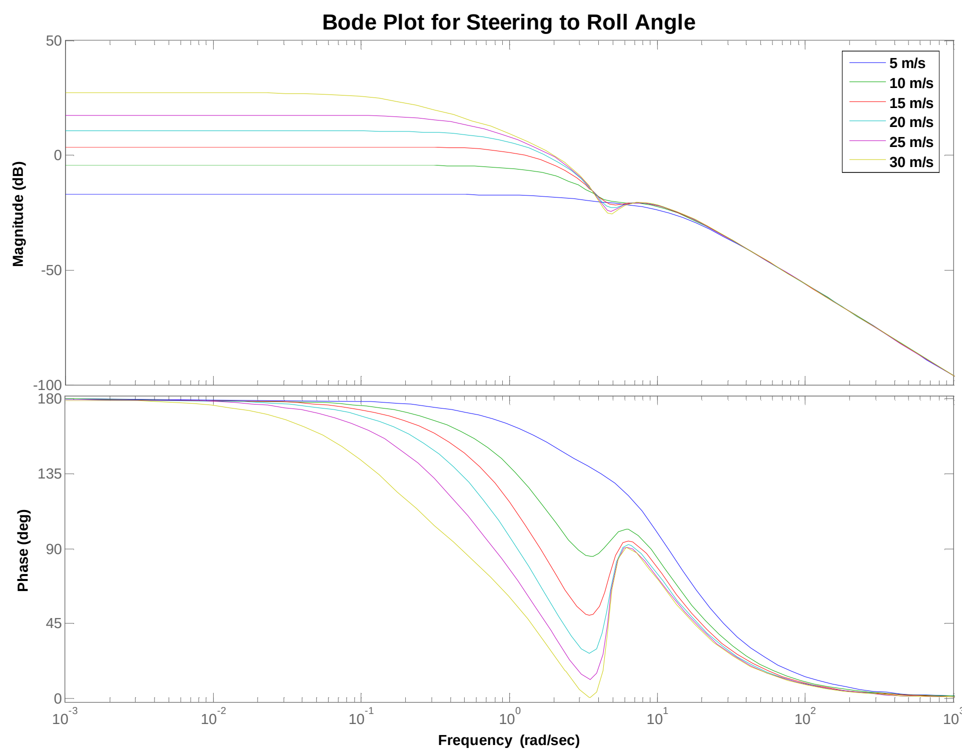

Figure **3-3**: Bode Diagram for Front Steering Input to Roll Angle for Roll Model

If tire slip is the desired output, Eq. **3.22** can be used as the output equation in the state space model. The Bode plots for front and rear tire slip are shown in Figure **3-4** and Figure **3-5**. The bicycle model and the roll model magnitudes are also compared in these figures for a velocity of 20 m/s. The models appear to match very well.

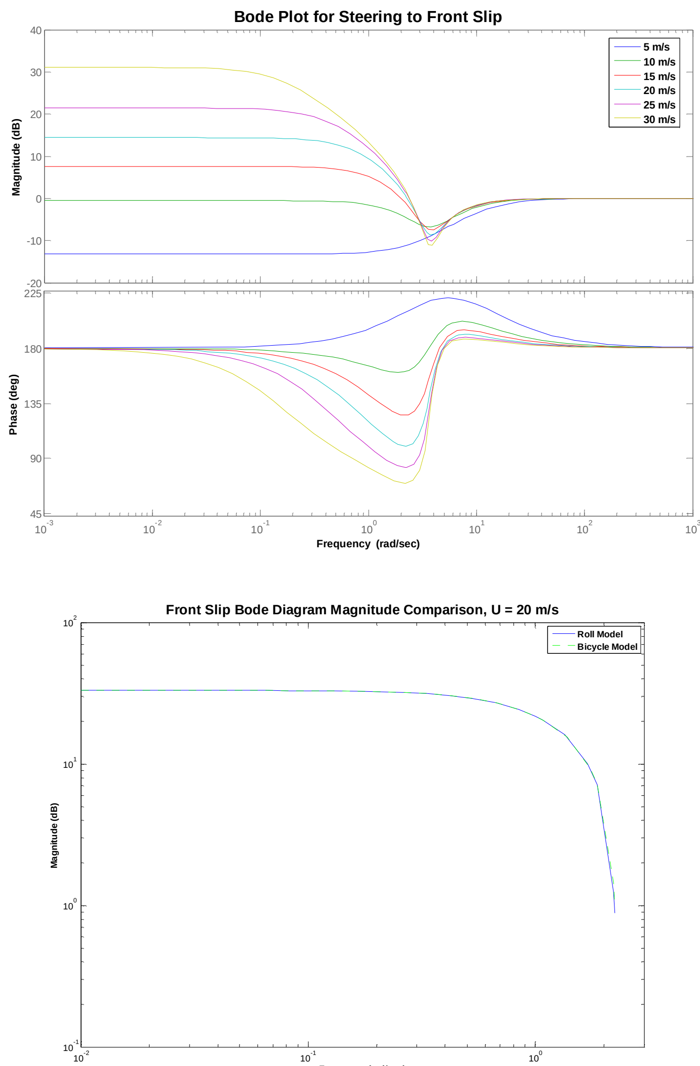

Figure **3-4**: Bode Diagram for Front Steering Input to Front Tire Slip Angle for the Roll Model and Comparison to Bicycle Model of Front Tire Slip at 20 m/s

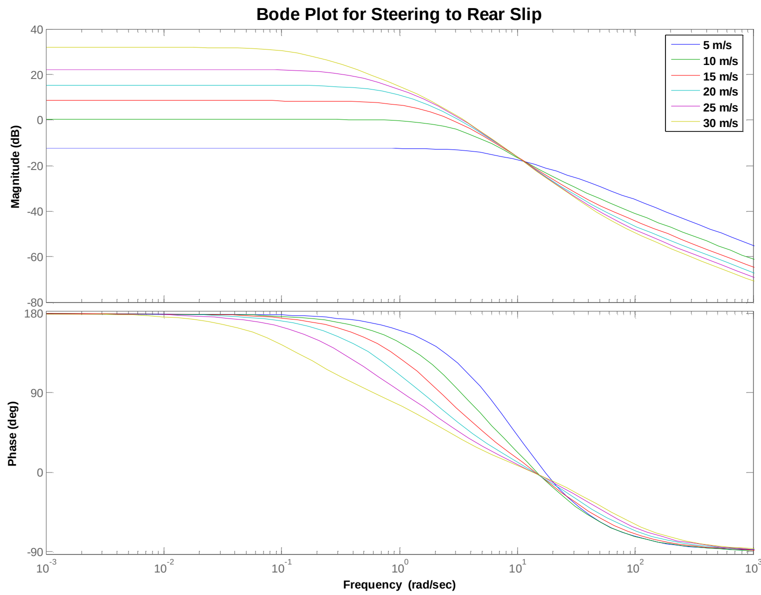

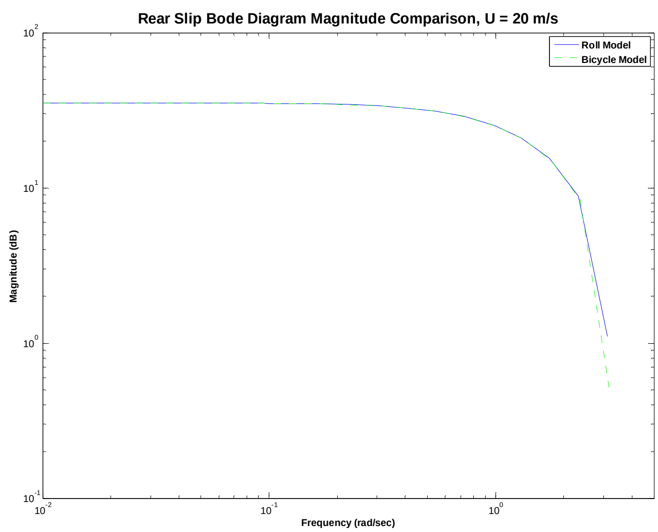

Figure **3-5**: Bode Diagram for Front Steering Input to Rear Tire Slip Angle for the Roll Model and Comparison to Bicycle Model of Rear Tire Slip at 20 m/s

Using the same method as the previous chapter, the maximum steering input before tire saturation can be plotted versus frequency to see which steering frequencies are most likely to cause slip as seen in Figure **3-6** and Figure **3-7** .

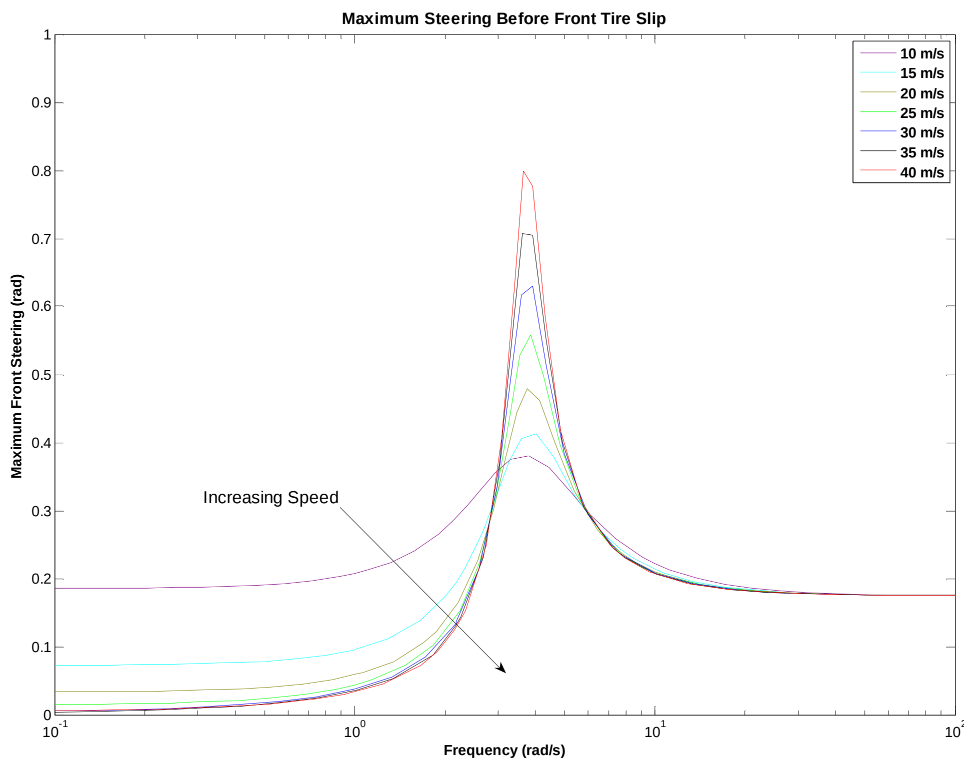

Figure **3-6**: Front Steering Input Which Causes Front Tire Saturation for the Roll Model

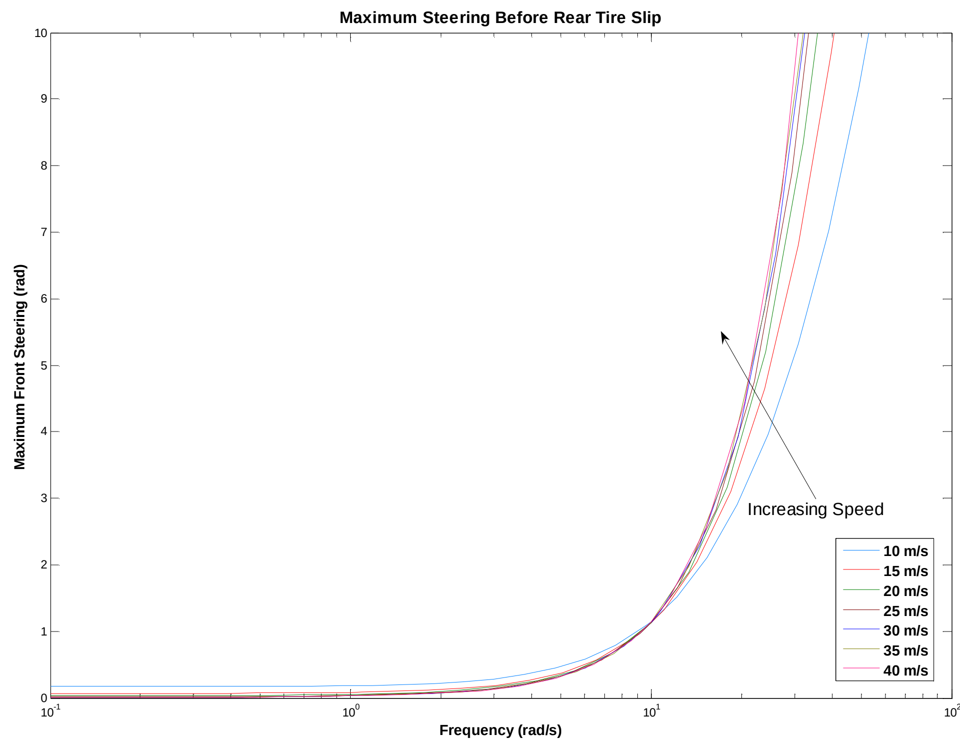

Figure **3-7**: Front Steering Input Which Causes Rear Tire Saturation for the Roll Model

3.1.2 Wheel Lift Threshold

In order to determine wheel lift, it is important to look at the restoring moment of the vehicle. The maximum restoring moment $M_{rest,\max}$ can be found using a simple force balance. The forces from the suspension on the wheels are shown in Figure **3-8**.

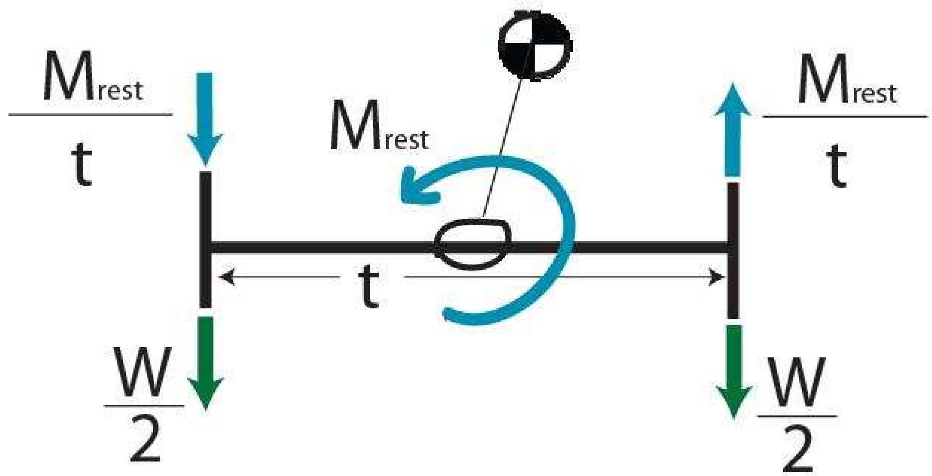

Figure **3-8**: Force Balance Between the Suspension and Wheels

The suspension provides the restoring moment. On the passenger tire, summing of the vertical forces results in:

$$\sum F = \frac{-M_{rest}}{t} + \frac{W}{2} \qquad \mathbf{3.24}$$

Therefore the threshold for wheel lift is:

$$M_{rest,\max} = \frac{W}{2} t \qquad \mathbf{3.25}$$

because the restoring moment will exceed the force from the weight of the vehicle if it is greater than the above value. The restoring moment can be found using the following output equation in the state-space model:

$$y_{restoring} = \begin{bmatrix} 0 & 0 & K_{\varphi} & D_{\varphi} \end{bmatrix} \cdot \begin{bmatrix} V \\ r \\ \phi \\ \dot{\phi} \end{bmatrix} + [0]\delta_f \qquad \mathbf{3.26}$$

The Bode plot for steering to restoring moment is shown in Figure **3-9**

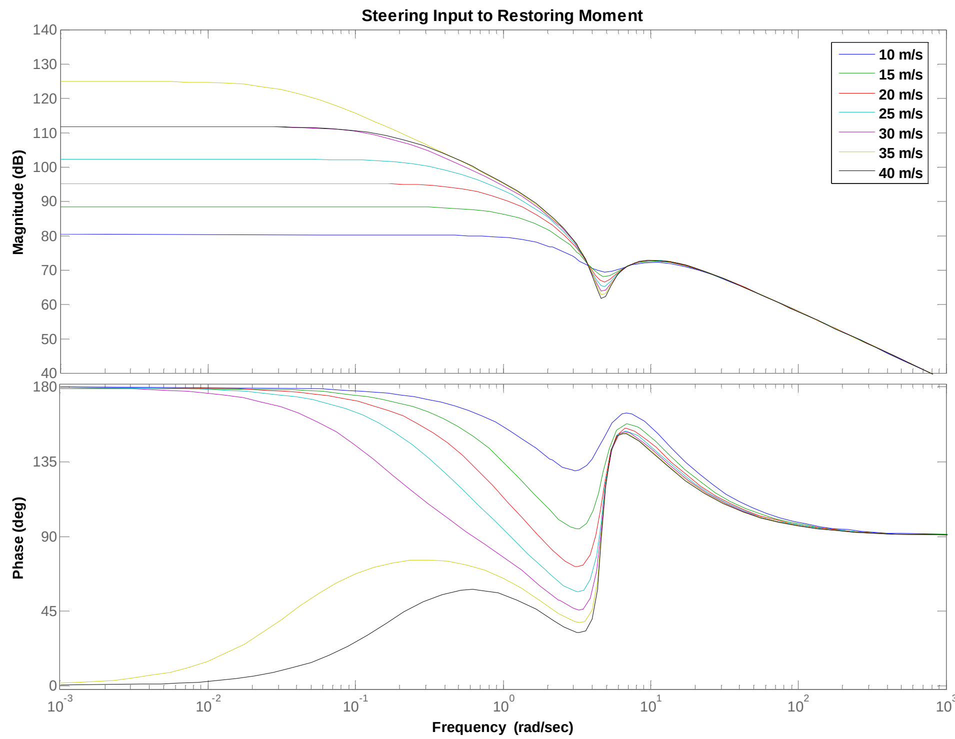

Figure **3-9**: Bode Diagram for Front Steering Input to Restoring Moment for the Roll Model

Using a similar method to the one used to find the steering input at tire saturation, the steering input at which wheel lift will occur can also be calculated. The Bode plot provides the ratio of restoring moment, M_{rest}, to steering input at a given frequency. The magnitude of the maximum steering angle before wheel lift, $\delta_{f,lift}$, can be calculated using the given ratio and the maximum restoring moment, $M_{rest,\max}$:

$$\delta_{f,lift} = \left(\frac{M_{rest}}{\delta_f} \right)^{-1} M_{rest,\max} \qquad \textbf{3.27}$$

Substituting the value in Eq. **3.25** into Eq. **3.27** allows the calculation of the maximum steering angle before wheel lift occurs. Figure **3-10** shows the maximum steering input before wheel lift as a function of frequency.

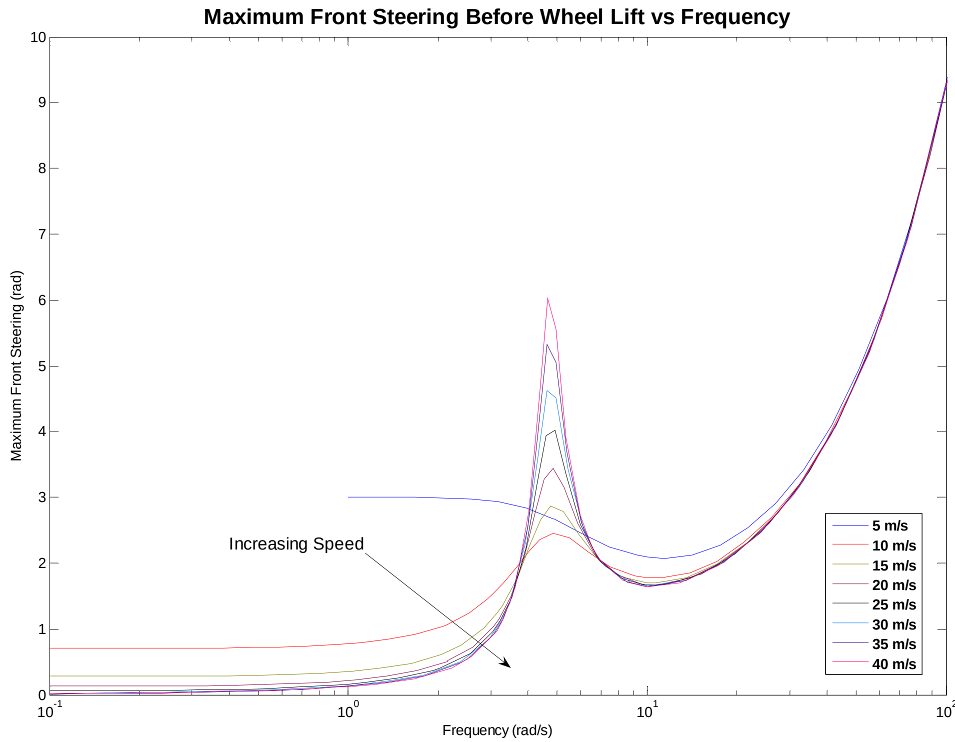

Figure **3-10**: Front Steering Input That Causes Wheel Lift for the Roll Model

The maximum steering before wheel lift can then be directly compared to the maximum steering before tire saturation. Using the vehicle parameters for a Mercury Tracer, the maximum steering angle for saturation and wheel lift were plotted together at various speeds in Figure **3-11**. As expected, the Tracer is much more likely to achieve tire saturation than wheel lift primarily due to its low CG height.

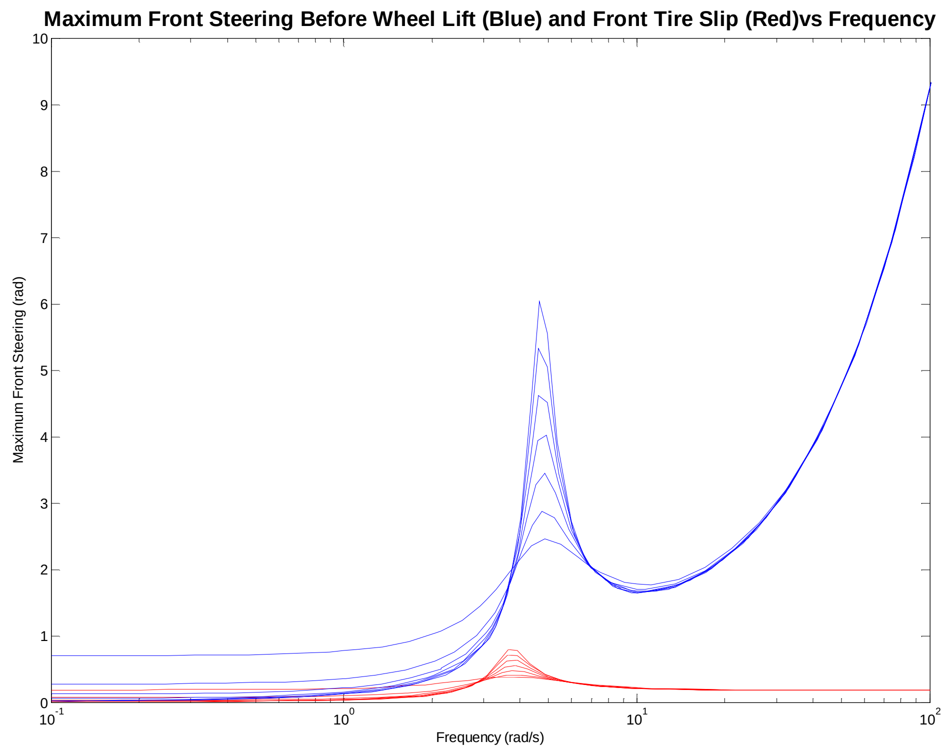

Figure **3-11**: Comparison of Maximum Steering Before Wheel Lift and Front Tire Slip for Mercury Tracer

A direct comparison of individual speeds is shown in Figure **3-12** and Figure **3-13**.

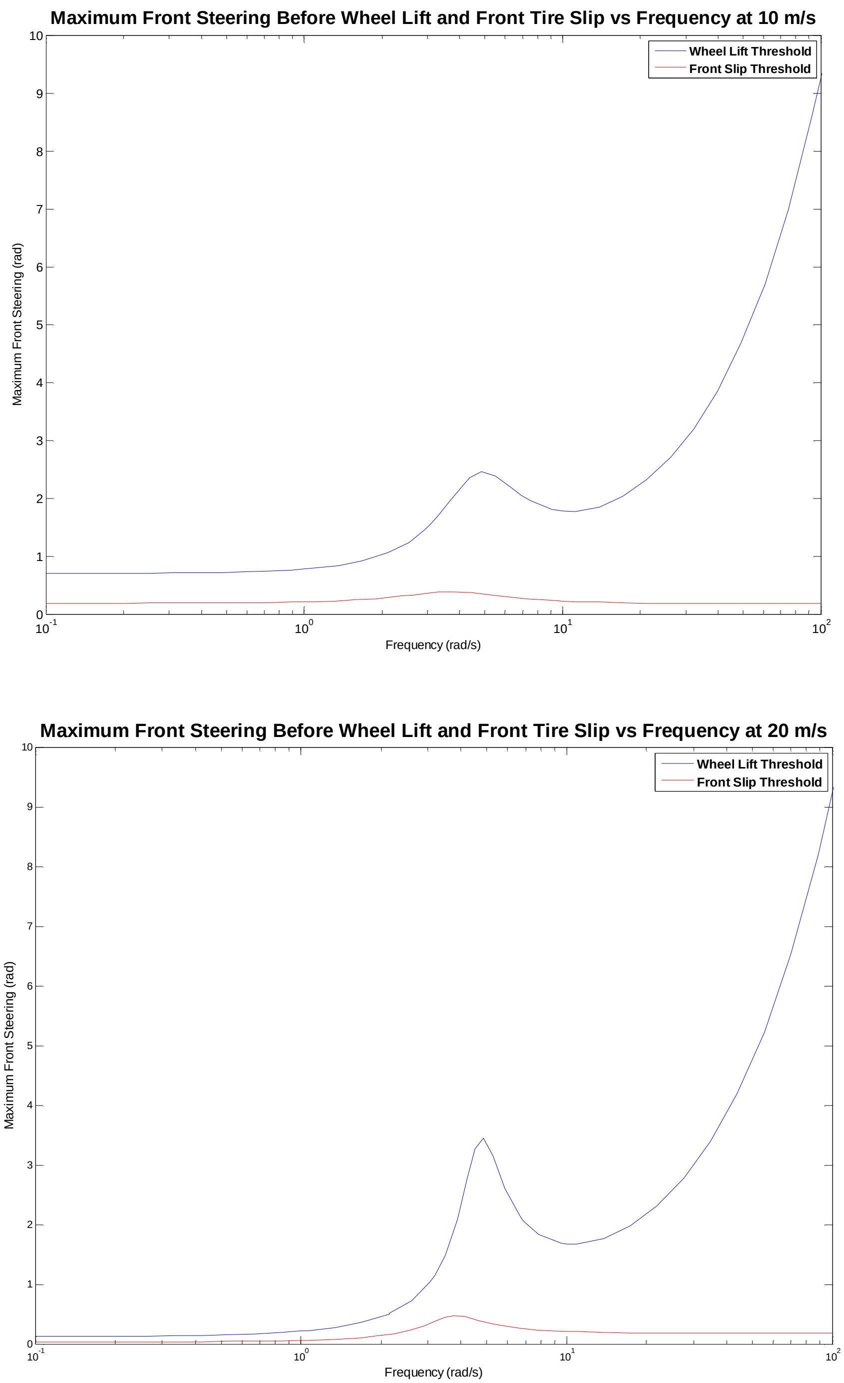

Figure **3-12**: Maximum Steering Before Wheel Lift and Tire Saturation for the Mercury Tracer at 10 m/s and 20 m/s

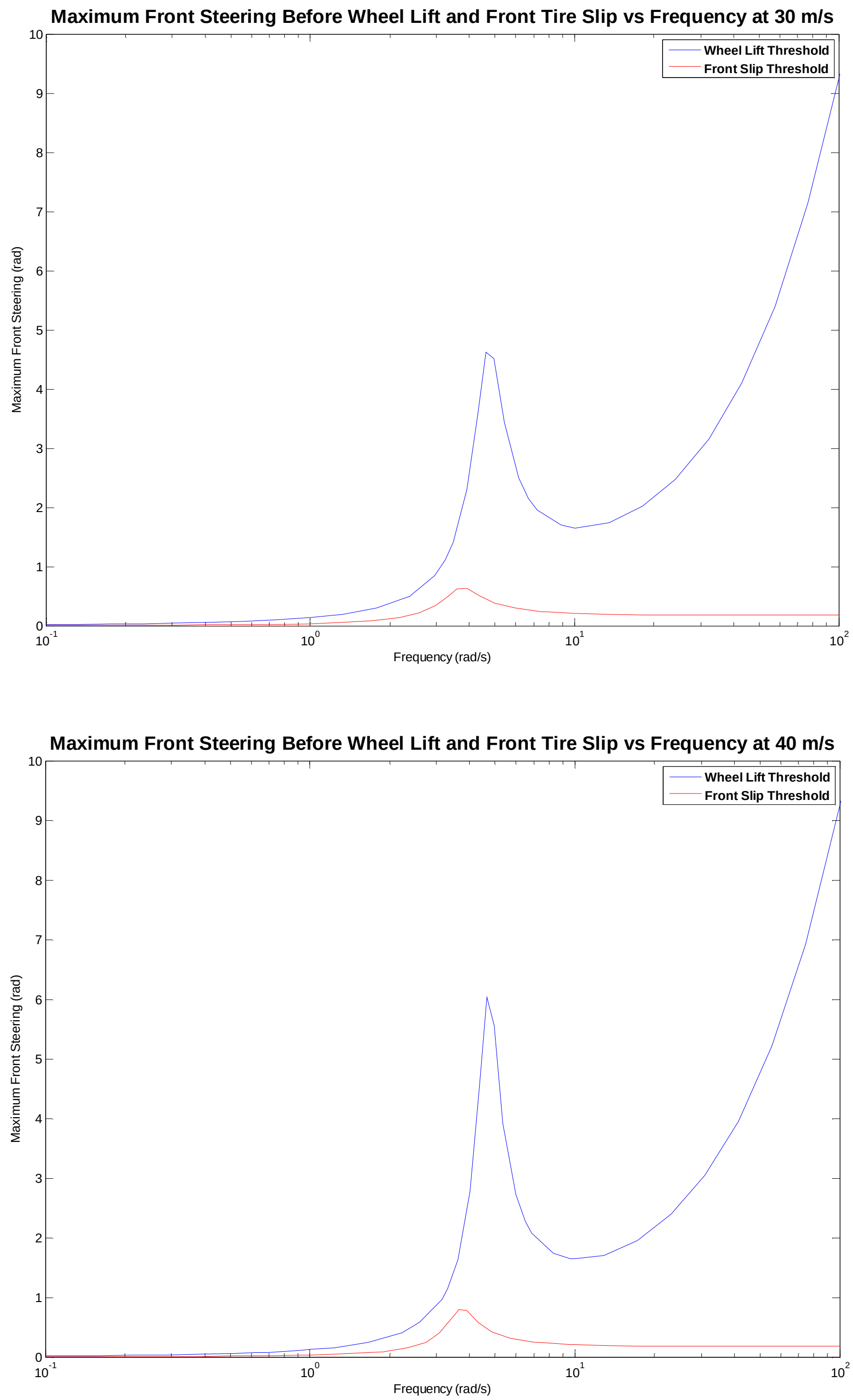

Figure **3-13**: Maximum Steering Before Wheel Lift and Tire Saturation for the Mercury Tracer at 30 m/s and 40 m/s

Using the parameters of a Jeep Grand Cherokee for further analysis, the following plots in Figure **3-14** and Figure **3-15** compare the maximum steering for wheel lift and tire saturation at various speeds for the Jeep.

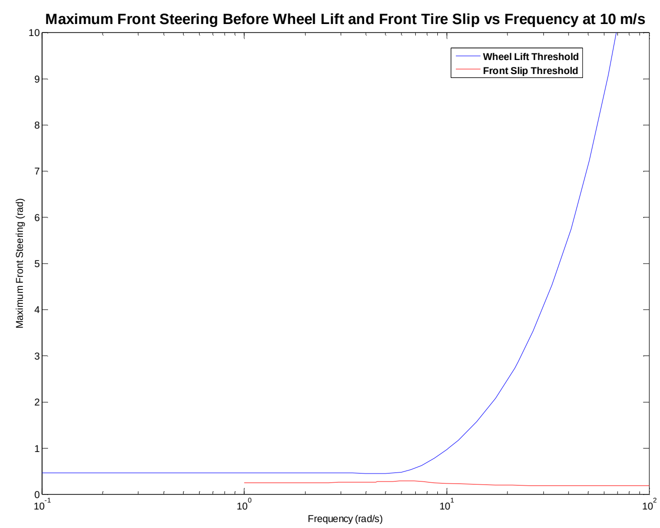

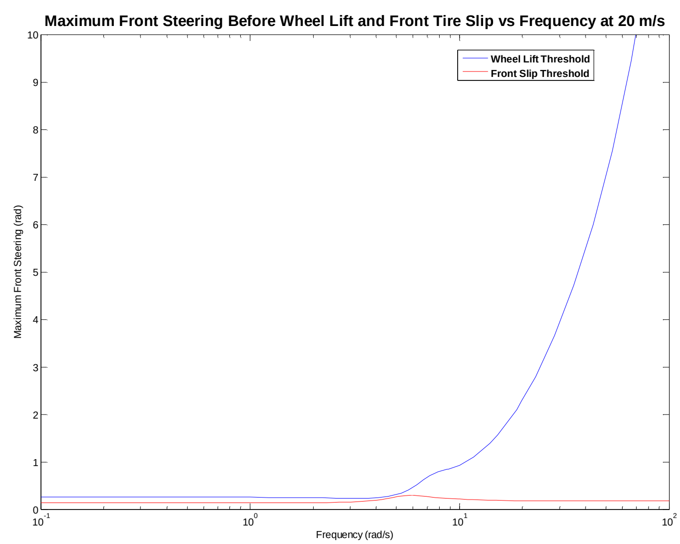

Figure **3-14**: Maximum Steering Before Wheel Lift and Tire Saturation for the Jeep Grand Cherokee at 10 m/s and 20 m/s

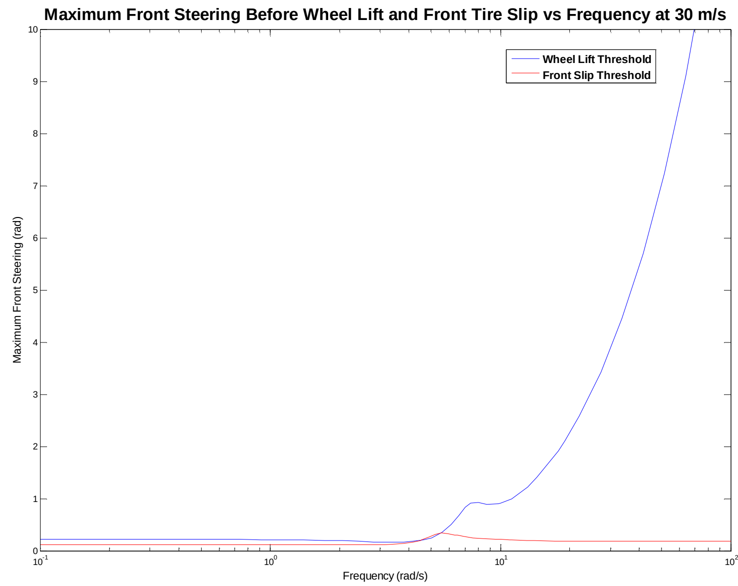

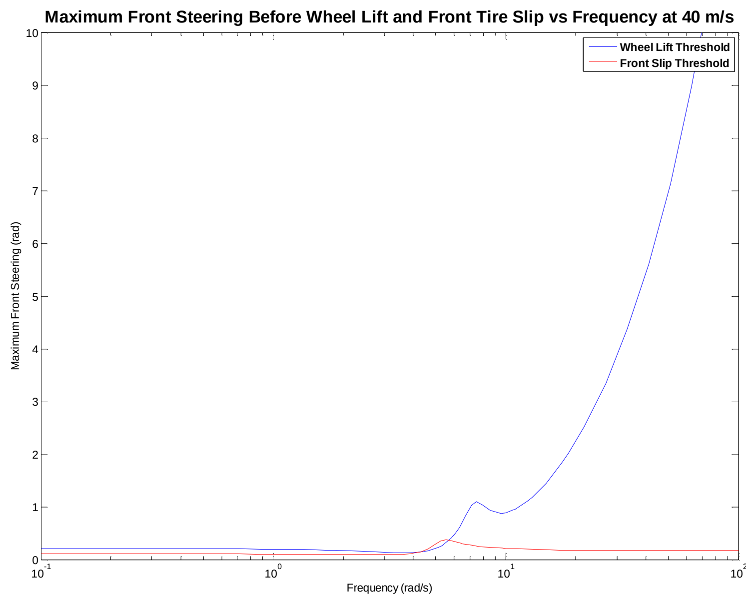

Figure **3-15**: Maximum Steering Before Wheel Lift and Tire Saturation for the Jeep Grand Cherokee at 30 m/s and 40 m/s

The Jeep is more likely to slip than achieve wheel lift at lower speeds, but it will experience wheel lift at higher speeds for a limited range of frequencies.

3.2 Conclusions

In this chapter, a roll model was derived using Newtonian mechanics. Unlike the bicycle model, the roll model has 3DOF. State-space models were used to demonstrate how front steering input affects roll angle, tire slip, and restoring moment. The maximum steering input before tire saturation was calculated for various frequencies and speeds using the same method that was used for the bicycle model. A similar method was used to calculate the maximum steering input before wheel lift based on the restoring moment from the suspension. The maximum steering input before slip and the maximum steering input before wheel lift were then directly compared for both the Mercury Tracer and the Jeep Grand Cherokee to predict whether the vehicles would slip before wheel lift, and hence rollover.

1. J.T. Cameron, "Vehicle Dynamic Modeling for the Prediction and Prevention of Vehicle Rollover," M.S. Thesis, Mechanical and Nuclear Engineering, Pennsylvania State University, Dec. 2005.

2. H.-J. Kim and Y.-P. Park, "Investigation of robust roll motion control considering varying speed and actuator dynamics," *Mechatronics*, 2003.

3. J.C. Dixon, *Tires, Suspension, and Handling*, 2^{nd} Ed. Warrendale, PA: The Society of Automotive Engineers (SAE), 1996.

4. J.H. Ginsberg, *Advanced Engineering Dynamics*, 2^{nd} ed. New York, NY: Cambridge University Press, 1998.

Chapter 4

Rollover Prevention Algorithm

In the previous chapter, the threshold for wheel lift was calculated for the Mercury Tracer and the Jeep Grand Cherokee. Neither vehicle was extremely susceptible to wheel lift since they were much more likely to experience tire saturation first. Other vehicles, such as SUVs, for example, are known to have problems with wheel lift. In this chapter, a feed-forward controller will be proposed to help prevent wheel lift. The parameters of the Mercury Tracer will be adjusted by adding a load at the top of the vehicle and reducing the damping rate in order to make the vehicle more likely to experience rollover. Then the new system will be subjected to an open-loop controller which will help reduce the restoring moment acting on the vehicle and therefore the likelihood of rollover.

4.1 Dead-Beat Control

The dead-beat control method was chosen for its simplicity [**1**]. In this open-loop control method, the goal is to replace the undesired dynamics of a system with those of a desired system. For demonstration, a simple system represented by the transfer function in Eq. **4.1** will be used. This damping ratio of this example system is 0.1.

$$\frac{y}{u} = \frac{s + 2.25}{s^2 + 0.15s + 2.25} = \frac{B(s)}{A(s)} \qquad \textbf{4.1}$$

If the output of this system was undesirable, one may wish to make it resemble an acceptable system. The system in Eq. **4.2** with a damping ratio of 0.9 will be used as the desirable system.

$$\frac{y}{u} = \frac{1}{s^2 + 1.35s + 2.25} = \frac{B_d(s)}{A_d(s)} \qquad \mathbf{4.2}$$

The dead-beat filter is then chosen so that it will completely cancel out the first system and replace it with the desired system. The complete system is shown in Figure **4-1** in block diagram format.

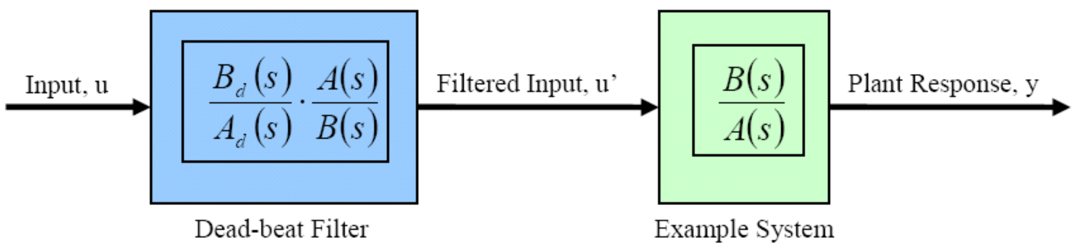

Figure **4-1**: Sample Dead-Beat Filter System

The system simplifies to the one shown in Figure **4-2** below.

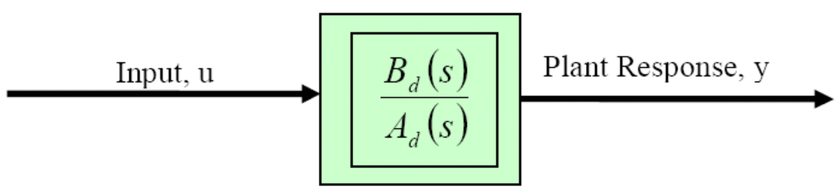

Figure **4-2**: Filtered System

In this example, the dead-beat filter would be:

$$\frac{u'}{u} = \frac{B_d(s) \cdot A(s)}{A_d(s) \cdot B(s)} = \frac{\left(s^2 + 0.15s + 2.25\right)}{\left(s^2 + 1.35s + 2.25\right)\left(s + 2.25\right)} = \frac{s^2 + 0.15s + 2.25}{s^3 + 3.6s^2 + 5.2875s + 5.0625} \qquad \mathbf{4.3}$$

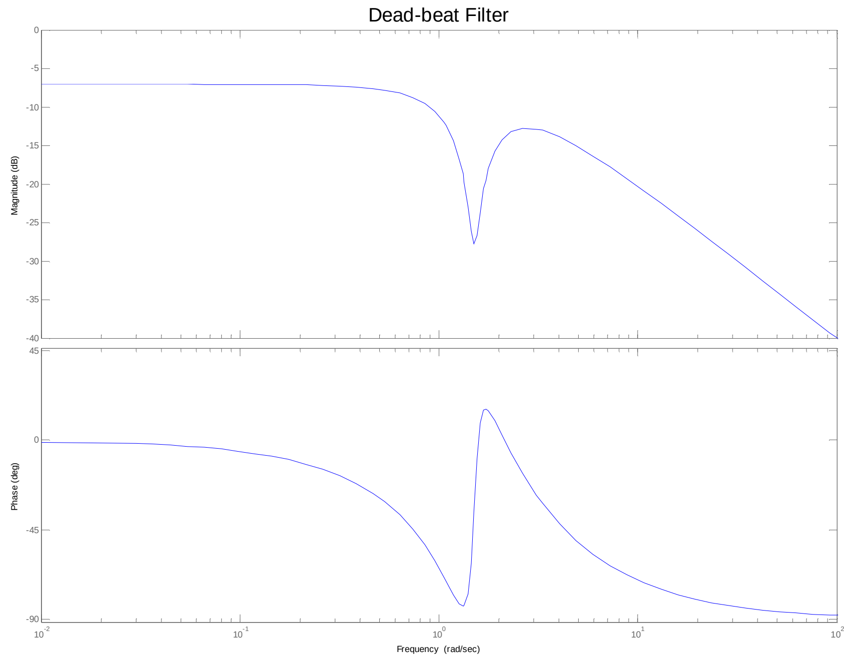

Figure **4-3**: Dead-Beat Filter

By applying the filter, the system dynamics clearly become more damped. Figure **4-4** shows the example system and the filtered system. Figure **4-5** shows a comparison of the filtered system and the desired system. As expected, the desired and filtered plots show the systems are identical.

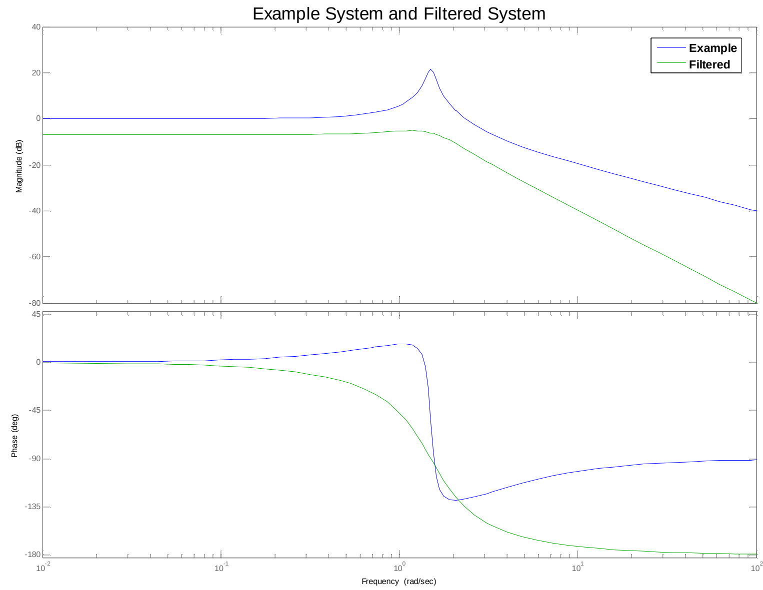

Figure **4-4**: Example System and Filtered System for Dead-Beat Controller

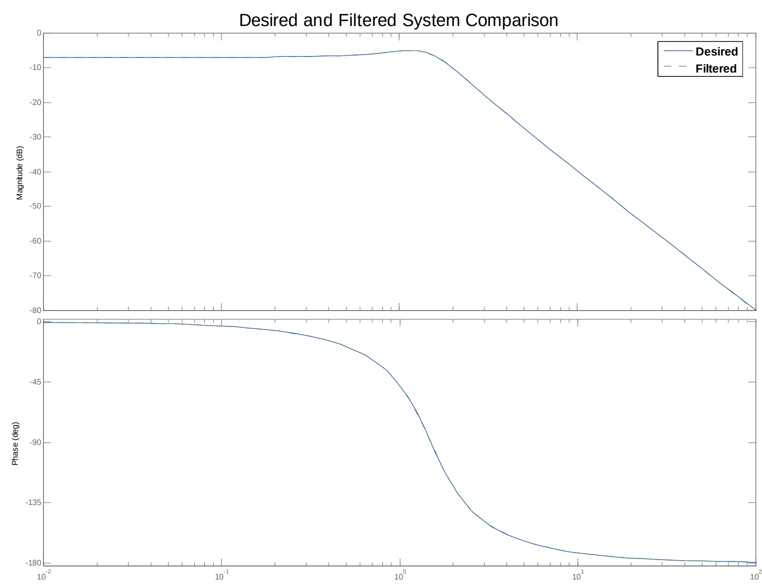

Figure **4-5**: Desired System and Filtered System for Dead-Beat Controller

The effects of the filter can also be seen in the time domain in Figure **4-6**

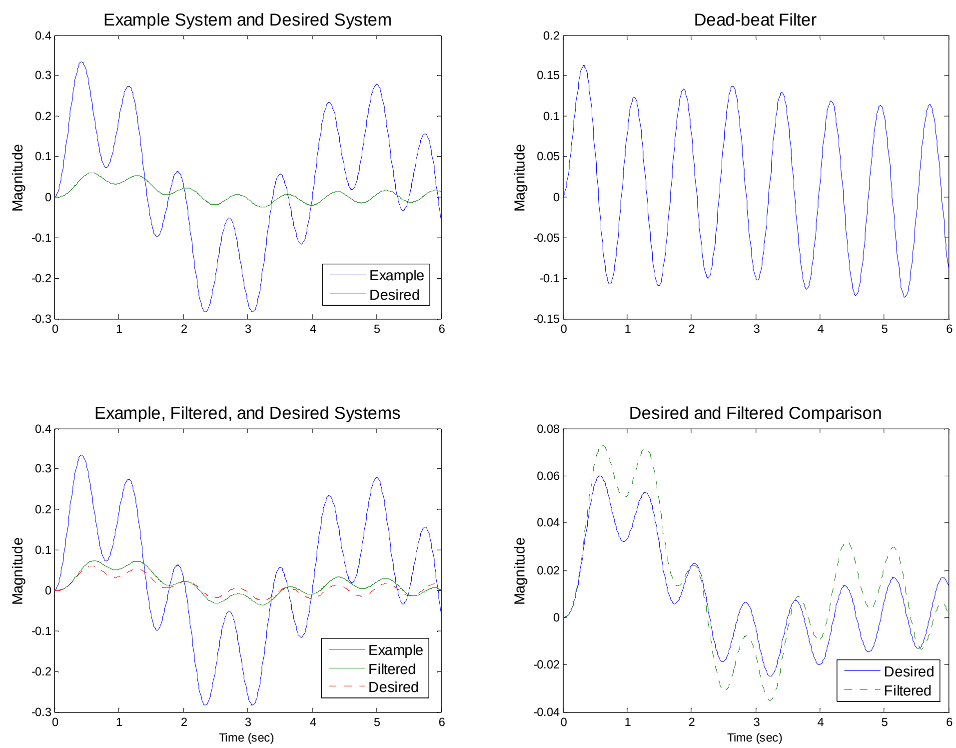

Figure **4-6**: Implementation of the Dead-Beat Filter on the Example System

4.2 Creating the High Roller

To demonstrate the use of the dead-beat controller on vehicle dynamics, a fictitious vehicle was created to implement the method used in Cameron's work [**2**]. First, the damping rate of the vehicle was reduced by forty percent. For the Mercury Tracer this resulted in a decrease of the roll damping from 5000 N-s/rad to 3000 N-s/rad. Then an imaginary load of 200 kg was added to the vehicle at a height of 2 meters. This increased the total mass of the vehicle, modified the value of I_{xx}, and increased the height of the center of gravity. The remaining parameters were unchanged. The modified vehicle will be referred to as the *High Roller* as it was referred to in Cameron's work. A comparison of the parameters is found in Table **4-1**.

Table **4-1**: Comparison of Mercury Tracer and High Roller Parameters

Parameter	Mercury Tracer	High Roller	Units
m	1031.92	1231.92	kg
m_s	825.5	985.5	kg
I_{zz}	1850.5	1850.5	kg-m^2
I_{yy}	1705	1705	kg-m^2
I_{xx}	375	456.25	kg-m^2
I_{xz}	72	72	kg-m^2
l_f	0.9271	0.9271	m
l_r	1.5621	1.5621	m
L	2.4892	2.4892	m
t	1.43	1.43	m
h	0.25	0.534	m
C_f	-83014	-83014	N/rad
C_r	-88385	-88385	N/rad
K_φ	17000	17000	N-m/rad
D_φ	5000	3000	N-s/rad

4.3 Implementation of Dead-Beat Controller

In this section the dead-beat controller is applied to the High Roller to reduce the wheel lift propensity. As shown in the previous chapter, wheel lift will occur when the restoring moment exceeds a certain value. By replacing the dynamics associated with the restoring moment of the High Roller with those of the Mercury Tracer, the dead-beat controller will help reduce the magnitude of the restoring moment and thereby prevent wheel lift from occurring.

The transfer function for the restoring moment as the output and the front steering as the input for the High Roller at 30 m/s is:

$$\frac{B(s)}{A(s)} = \frac{-246700s^3 - 2926000s^2 - 37990000s - 16620000}{s^4 + 19.18s^3 + 162.4s^2 + 653.1s + 1515} \qquad \textbf{4.4}$$

The desired dynamics are those of the Mercury Tracer with the corresponding transfer function:

$$\frac{B_d(s)}{A_d(s)} = \frac{-215400s^3 - 2066000s^2 - 30150000s - 87090000}{s^4 + 24.28s^3 + 240.1s^2 + 1188s + 2311} \qquad \textbf{4.5}$$

Therefore, the dead-beat filter is:

$$\frac{u'}{u} = \frac{2.154\times10^5 s^7 + 6.199\times10^6 s^6 + 1.048\times10^8 s^5 + 1.142\times10^9 s^4 + 8.243\times10^9 s^3 + 3.697\times10^{10} s^2 + 1.025\times10^{11} s + 1.319\times10^{11}}{2.467\times105s^7 + 8.915\times10^6 s^6 + 1.683\times10^8 s^5 + 2.084\times10^9 s^4 + 1.72\times10^{10} s^3 + 9.18\times10^{10} s^2 + 2.853\times10^{11} s + 3.842\times10^{11}} \qquad \textbf{4.6}$$

The roll moment response of the High Roller, for a sinusoidal steering input, shown in Figure **4-7** is reduced to that of the Mercury Tracer. The roll moment response is also reduced for a pseudo-step input as shown in Figure **4-8**.

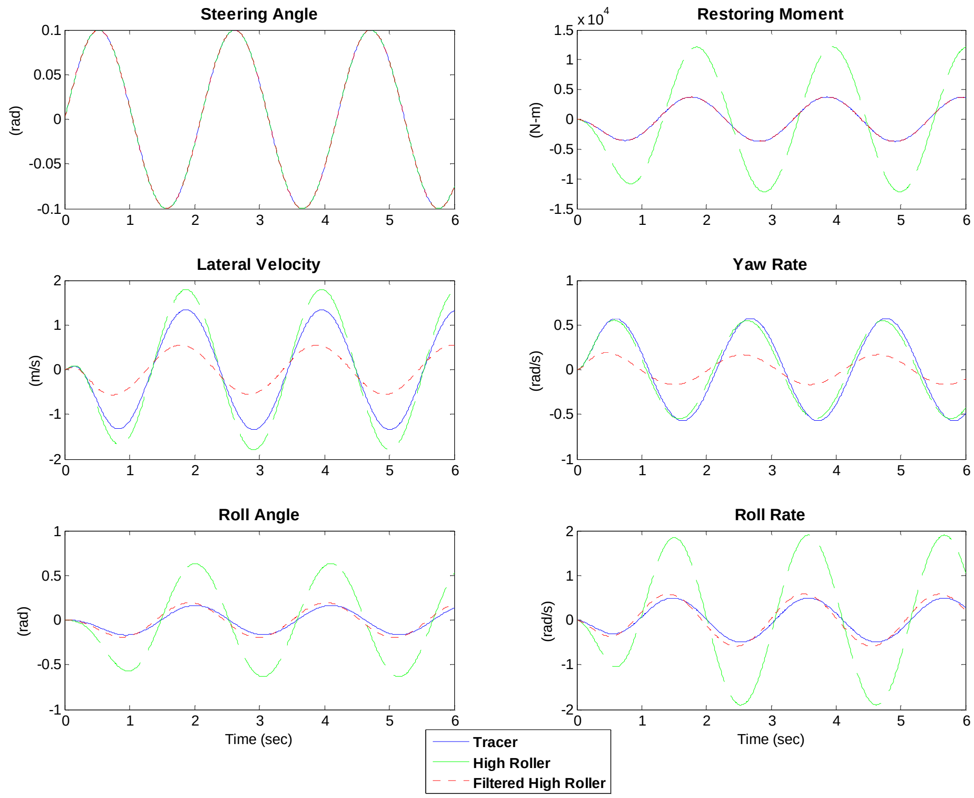

Figure **4-7**: Comparison of the Tracer, High Roller, and Filtered High Roller Dynamics, Sinusoidal Excitation, 8.2 rad/s, 0.1 rad Amplitude at 30 m/s

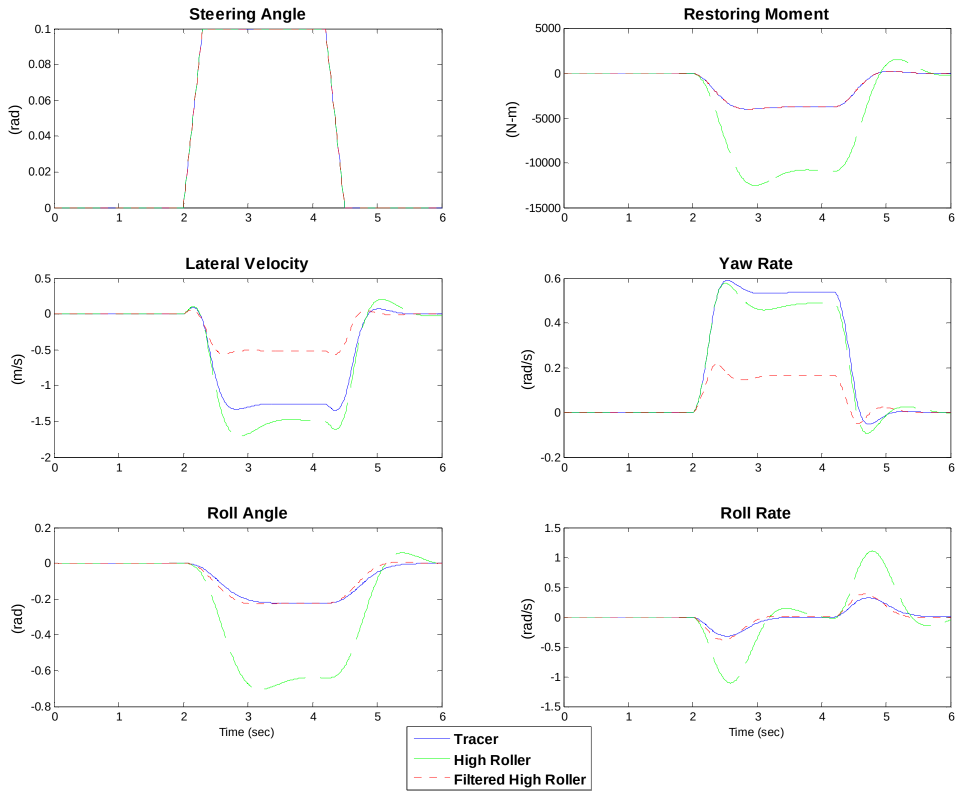

Figure **4-8**: Comparison of the Tracer, High Roller, and Filtered High Roller Dynamics, Pseudo-Step Input, 0.1 rad Amplitude at 30 m/s

It appears that the dead-beat controller is very effective in preventing rollover, and it is certainly very easy to design. The controller, however, requires perfect model knowledge [**2**]. Unfortunately, this is not realistic in the real world, but it may still be effective for a practical model. This issue is not the direct focus of this work, but issues of model uncertainty are discussed further in Cameron’s thesis and the interested reader is referred there for details [**2**].

4.4 Conclusions

The dead-beat controller is a great option for rollover mitigation due to its simplicity. In this chapter, it was successfully used to reduce the restoring moment experienced by the High Roller. In the next chapter, a dead-beat filter will be used to help prevent rollover for a vehicle traveling on a banked surface.

1. S. Skogestad and I. Postlethwaite, *Multivariable Feedback Control, Analysis and Design*, West Sussex, England: John Wiley & Sons Ltd., 1996.

2. J.T. Cameron, "Vehicle Dynamic Modeling for the Prediction and Prevention of Vehicle Rollover," M.S. Thesis, Mechanical and Nuclear Engineering, Pennsylvania State University, Dec. 2005.

Chapter 5

Rollover Prevention on a Banked Surface

In the previous chapters, the conditions for wheel lift were explored and a control algorithm was implemented to help prevent rollover at the same conditions. The thresholds for tire saturation and wheel lift as a function of steering were calculated to determine when slip would occur before wheel lift. If the surface of the road is not flat, it is expected that the threshold for wheel lift will decrease with an increase in bank angle. In this chapter, the conditions leading to wheel lift on a banked surface will be explored. Then the dead-beat control method will be implemented to prevent wheel lift under these new conditions.

5.1 Wheel Lift Threshold on a Banked Surface

First, the wheel lift threshold must be recalculated for the banked surface. As in Chapter 3, the maximum steering angle before wheel lift can be calculated using the maximum restoring moment. Using Figure **5-1** below, the maximum restoring moment can be calculated using the force balance in Eq. **5.1** for a surface banked at an angle of θ.

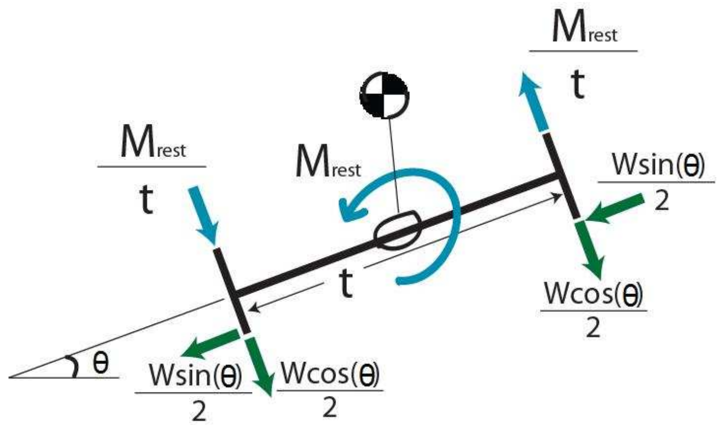

Figure **5-1**: Force Balance Between the Suspension and Wheels on Banked Surface

$$\sum F = \frac{-M_{rest}}{t} + \frac{W\cos(\theta)}{2} \quad \textbf{5.1}$$

Therefore, the threshold for wheel lift is:

$$M_{rest,\max} = \frac{W\cos(\theta)}{2} t \quad \textbf{5.2}$$

For the following calculations, the system is assumed to still be in linear operation at the banked angle. When calculating the frequency response, left and right turning maneuvers were not differentiated between. In reality, the equations for the moment required for wheel lift will be different for the uphill or downhill sides. Substituting the value found in Eq. **5.2** into the previous Eq. **3.27**, the maximum steering angle can be plotted for various values of θ. The maximum steering angle for wheel lift and tire saturation at 10 m/s versus frequency is shown in Figure **5-2**. As expected, the minimum steering input required for wheel lift decreases as the angle of the banked surface increases. An increase in speed of the vehicle also decreases the steering input required for wheel lift.

The difference in maximum steering input before wheel lift for different speeds can be seen in Figure **5-3** which compares the threshold for 10 m/s and 40 m/s.

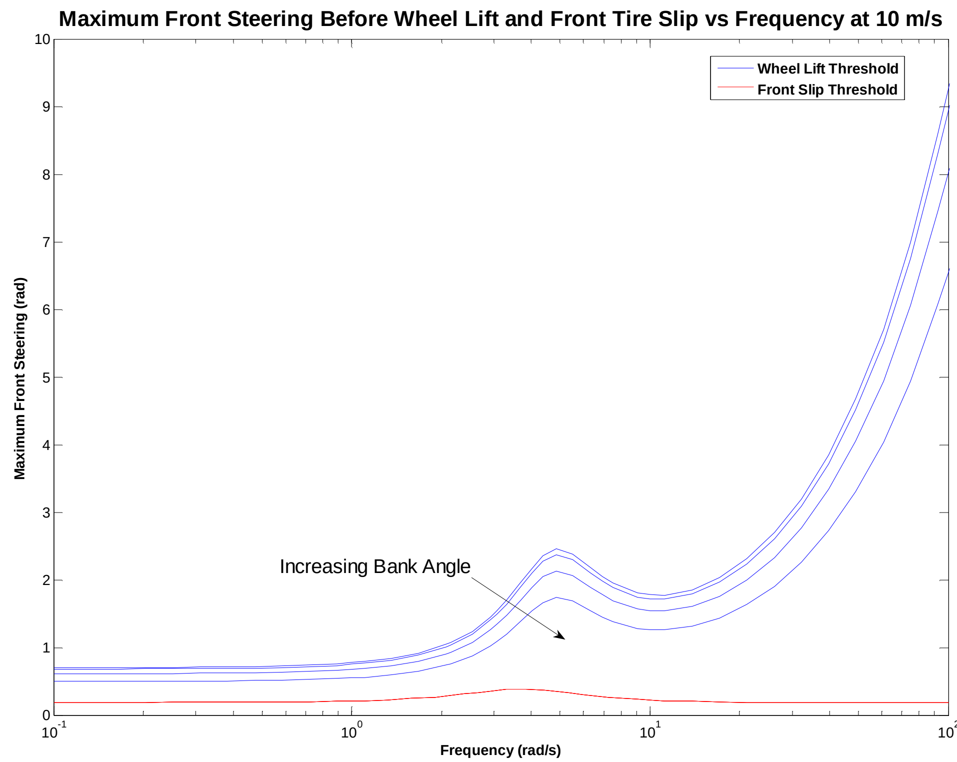

Figure **5-2**: Front Steering Input that Causes Wheel Lift and Tire Saturation for Various Bank Angles at 10 m/s

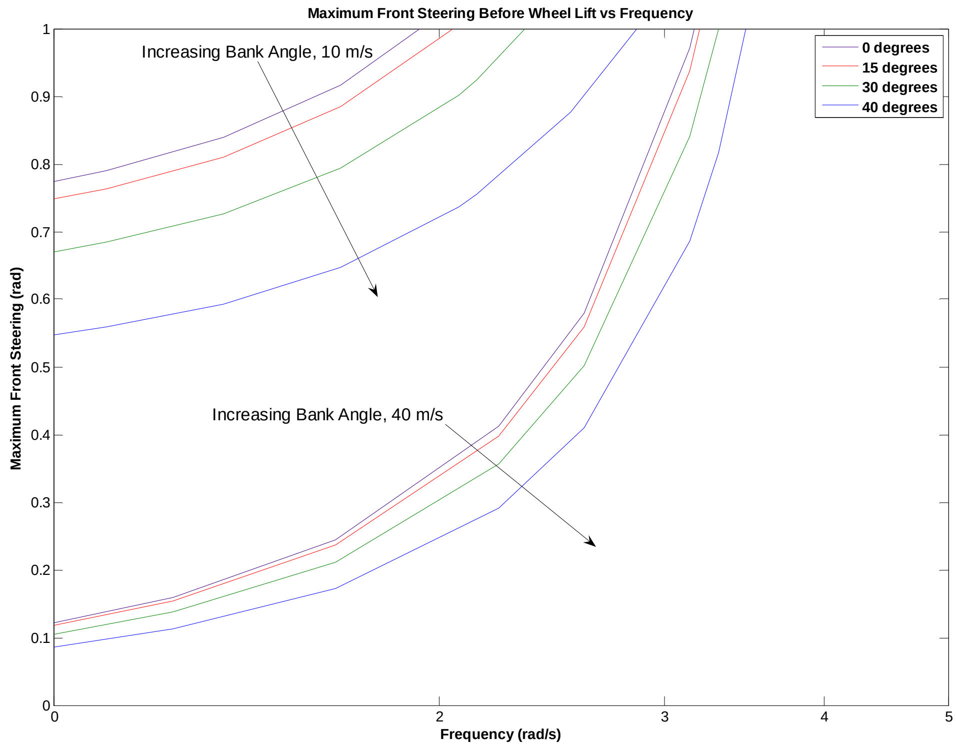

Figure **5-3**: Front Steering Input that Causes Wheel Lift for Various Bank Angles at 10 m/s and 40 m/s

The Tracer will still experience tire saturation at high bank angles and high speeds as shown in Figure **5-4** for a bank angle of 25 degrees and a speed of 40 m/s.

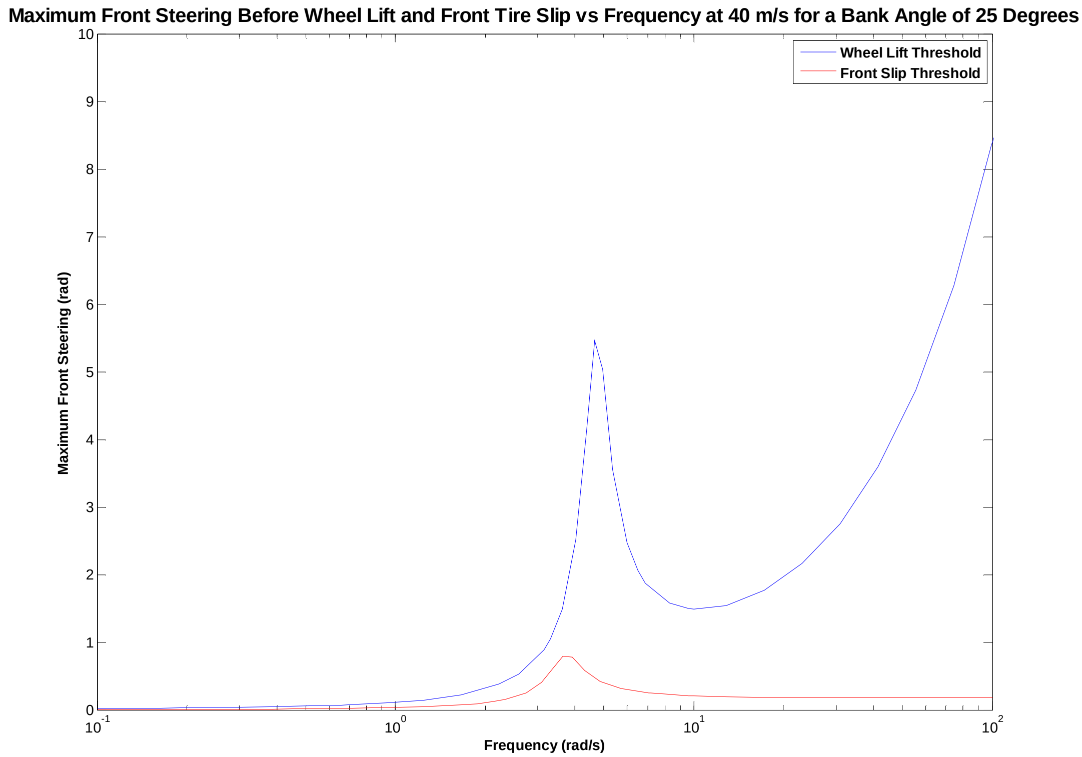

Figure **5-4**: Thresholds for Wheel Lift and Tire Saturation for the Tracer at High Speed of 40 m/s and a Banked Surface Angle of 25 Degrees

If the High Roller, however, is subjected to the same conditions, wheel lift will occur before tire saturation for a certain range of frequencies. In fact, the High Roller will experience wheel lift before tire saturation at 20 m/s at a bank angle of 25 degrees. Figure **5-5** shows the thresholds for wheel lift for the High Roller at these two conditions.

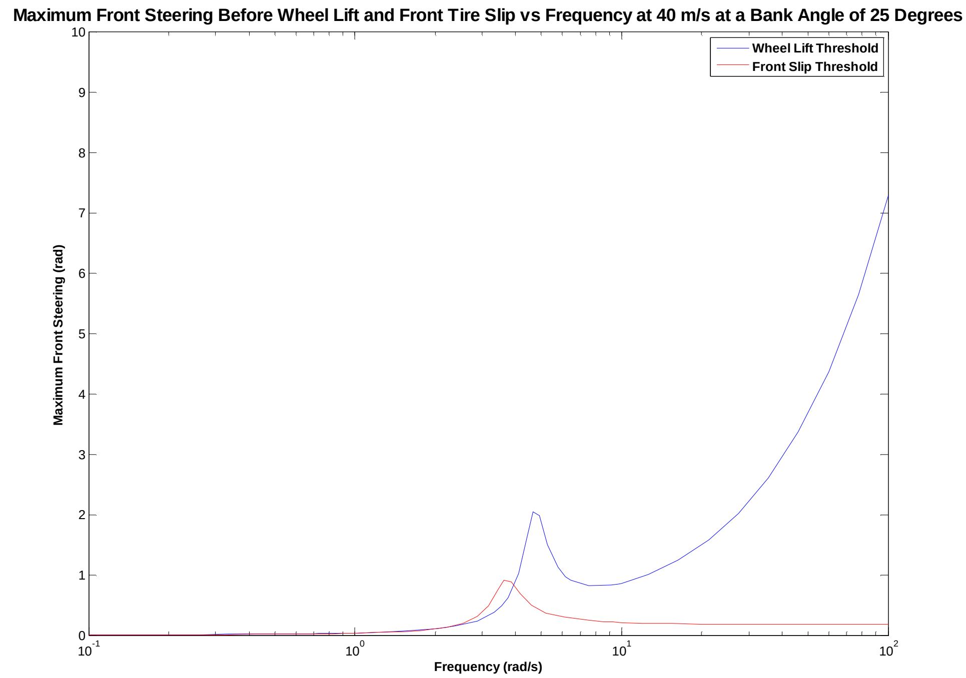

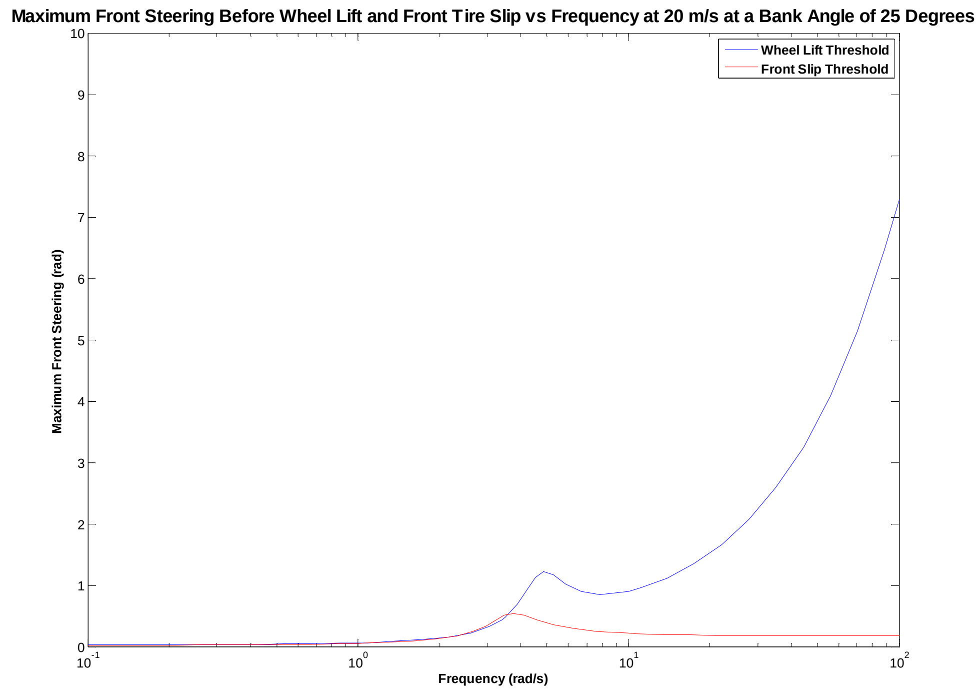

Figure **5-5**: Thresholds for Wheel Lift and Tire Saturation for the High Roller at Speeds of 40 m/s and 20 m/s and a Banked Surface Angle of 25 Degrees.

For both vehicles, an increase in bank angle clearly reduces the steering angle for wheel lift as expected. For the High Roller, however, an increased bank angle will cause wheel lift to occur before tire saturation.

5.2 Implementation of Dead-Beat Controller on a Banked Surface

Now the dead-beat controller will be applied to the High Roller on a banked surface to prevent wheel lift. In Figure **5-5**, the High Roller experiences wheel lift before tire saturation at a speed of 20 m/s and a bank angle of 25 degrees around a frequency input of 3 rad/s. The Mercury Tracer will experience tire saturation before wheel lift at the same conditions. Therefore, the Mercury Tracer will be used as the desired system again for the dead-beat control method.

The transfer functions for the High Roller and the Mercury Tracer at 20 m/s are shown in Eq. **5.3** and Eq. **5.4** respectively. The bank angle is only used to calculate the maximum restoring moment before wheel lift, so the transfer functions do not change with respect to bank angle.

$$\frac{B(s)}{A(s)} = \frac{-90000s^3 - 665200s^2 - 2856000s - 11220000}{s^4 + 11.62s^3 + 56.74s^2 + 114.5s + 54} \qquad \textbf{5.3}$$

$$\frac{B_d(s)}{A_d(s)} = \frac{-78670s^3 - 402500s^2 - 2188000s - 5.877000}{s^4 + 17.26s^3 + 94.35s^2 + 191s + 101.8} \qquad \textbf{5.4}$$

Therefore, the dead-beat filter is:

$$\frac{u'}{u} = \frac{7.867\times10^4 s^7 + 1.317\times10^6 s^6 + 1.133\times10^7 s^5 + 6.315\times10^7 s^4 + 2.428\times10^8 s^3 + 6.057\times10^8 s^2 + 7.911\times10s^8 + 3.174\times10^8}{9.009\times10^4 s^7 + 2.22\times10^6 s^6 + 2.284\times10^7 s^5 + 1.405\times10^8 s^4 + 5.993\times10^8 s^3 + 1.672\times10^9 s^2 + 2.434\times10s^9 + 1.142\times10^9} \qquad \textbf{5.5}$$

For a sinusoidal input at frequency of 3 rad/s with amplitude of 0.1 rad at a speed of 20 m/s, the filter successfully reduces the restoring moment of the High Roller to that of the Mercury Tracer. The results of this example are shown in Figure **5-6**.

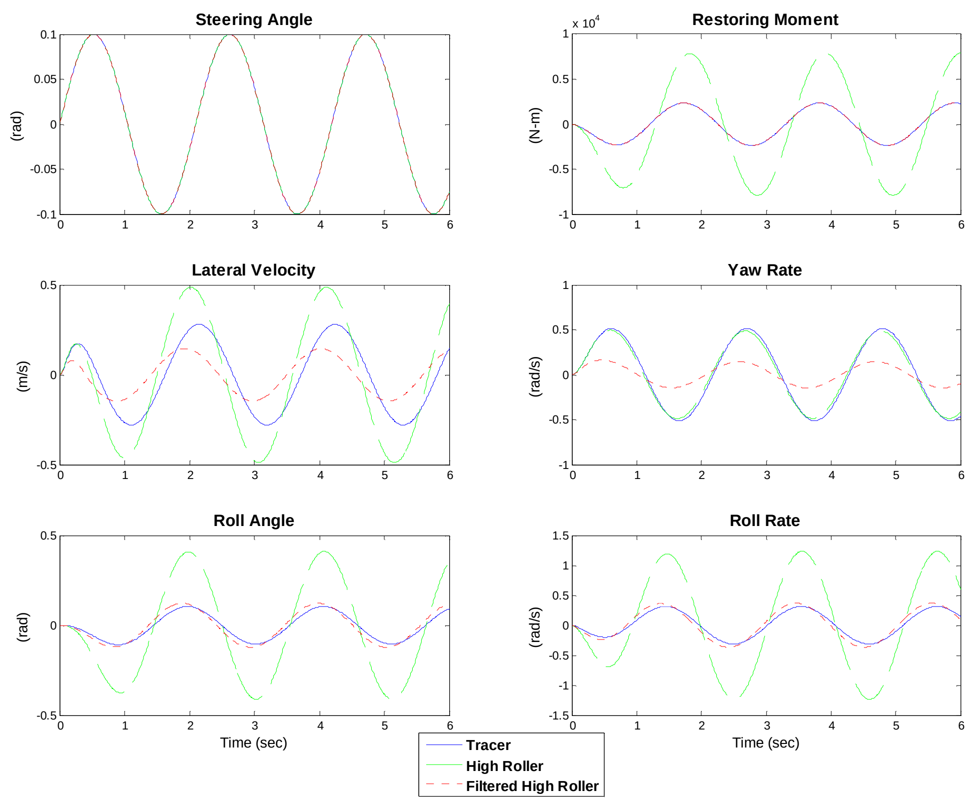

Figure **5-6**: Comparison of the Tracer, High Roller, and Filtered High Roller Dynamics, Sinusoidal Excitation, 3 rad/s, 0.1 rad Amplitude at U = 20 m/s

For a pseudo-step input at the same amplitude of 0.1 rad and at the same speed of 20 m/s, the restoring moment of the High Roller is again reduced to that of the Mercury Tracer as shown in Figure **5-7**.

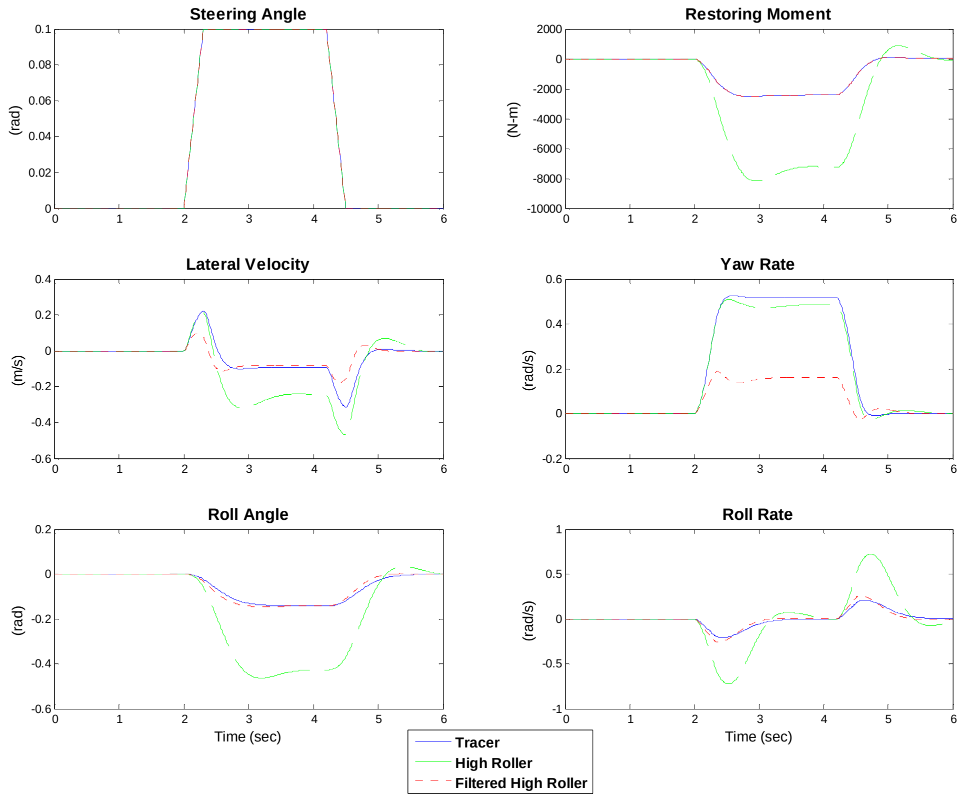

Figure **5-7**: Comparison of the Tracer, High Roller, and Filtered High Roller Dynamics, Pseudo-Step Input, 0.1 rad Amplitude at U = 20 m/s

5.3 Developing the Scaled Vehicle Controller

In the previous section, the High Roller was subjected to a filter to change the dynamics of the desired dynamics of the Mercury Tracer. A banked surface, however, can trip rollover for vehicles that are not usually susceptible to rollover. In the next chapter, wheel lift will be induced for a scale-sized vehicle similar to the Mercury Tracer by creating aggressive steering inputs on a banked surface. The scaled vehicle simulation model does not use the same body-fixed coordinates that were used to develop the previous control algorithm. Instead, it is based on an error-coordinate system. This system is convenient for running the scaled vehicle in order to help stabilize the yaw angle of the vehicle. The model was developed in previous work of the research group. Two additional variables are added to the state vector of this model shown in Eq. **5.6**. The state-variables are lateral velocity, lateral acceleration, yaw angle, yaw rate, roll angle, and roll rate respectively.

$$x = \begin{bmatrix} y & \dot{y} & \psi & \dot{\psi} & \phi & \dot{\phi} \end{bmatrix} \qquad \textbf{5.6}$$

The output equation for restoring moment is then:

$$y_{restoring} = \begin{bmatrix} 0 & 0 & 0 & 0 & K_{\varphi} & D_{\varphi} \end{bmatrix} \cdot \begin{bmatrix} y \\ \dot{y} \\ \psi \\ \dot{\psi} \\ \phi \\ \dot{\phi} \end{bmatrix} + [0]\delta_f \qquad \textbf{5.7}$$

Instead of creating a fictitious vehicle that is likely to experience rollover like the High Roller, this time an ideal vehicle which is less likely to experience rollover will be developed. Although the scaled vehicle resembles the Tracer which is not likely to rollover even at a banked angle, the ideal vehicle method was chosen to increase the effect of the controller. Furthermore, an algorithm based on an ideal vehicle could be used for a vehicle that does not normally experience rollover but may do so in a tripped situation such as driving on a banked surface. First, the CG of the vehicle will be lowered. Furthermore, the roll damping is increased for added rollover prevention. Using the scaled vehicle and ideal vehicle parameters in Table **5-1**, the transfer functions for restoring moment as the output can be calculated for both. The following controller is calculated for an example longitudinal velocity of 2.866 m/s because the scaled vehicle model was formulated at the same speed. It is interesting to note that the calculation of each transfer function is not dependent on the bank angle of the surface. The transfer functions only depend on the speed of the vehicle in addition to its parameters.

Table **5-1**: Scaled Vehicle and Ideal Vehicle Parameters

Parameter	Scaled Vehicle	Ideal Vehicle	Units
m	11.4	11.4	kg
ms	11.4	11.4	kg
Izz	1.2766	1.2766	kg-m^2
Ixx	0.1843	0.1843	kg-m^2
Ixz	0	0	kg-m^2
lf	0.240	0.240	m
lr	0.415	0.415	m
L	0.655	0.655	m
t	0.369	0.369	m
h	0.138	0.0874	m
Cf	-219.59	-219.59	N/rad
Cr	-304.76	-304.76	N/rad
Kφ	239.12	239.12	N-m/rad
Dφ	11	25	N-s/rad

The transfer function for the scaled vehicle is:

$$\frac{B(s)}{A(s)} = \frac{\left(-0.0002s^5 - 0.0116s^4 - 0.2489s^3 - 1.7786s^2\right)\cdot 1\times10^{-7}}{\left(0.0011s^5 + 0.0389s^4 + 0.6047s^3 + 3.7512s^2\right)\cdot 1\times10^{-7}} \quad \textbf{5.8}$$

The transfer function for the ideal vehicle is:

$$\frac{B_d(s)}{A_d(s)} = \frac{\left(-0.0026s^5 - 0.1054s^4 - 1.4860s^3 - 6.8501s^2\right)\cdot 1\times10^{-6}}{\left(0.0017s^5 + 0.0543s^4 + 0.6415s^3 + 2.6329s^2\right)\cdot 1\times10^{-5}} \quad \textbf{5.9}$$

The dead-beat controller can then be found as in the previous sections:

$$\frac{u'}{u} = \frac{2.86\times10^{-19}s^{10} + 2.171\times10^{-17}s^9 + 7.307\times10^{-16}s^8 + 1.388\times10^{-14}s^7 + 1.56\times10^{-13}s^6 + 9.717\times10^{-13}s^5 + 2.57\times10^{-12}s^4}{3.4\times10^{-19}s^{10} + 3.058\times10^{-17}s^9 + 1.181\times10^{-15}s^8 + 2.451\times10^{-14}s^7 + 2.868\times10^{-13}s^6 + 1.796\times10^{-12}s^5 + 4.683\times10^{-12}s^4} \quad \textbf{5.10}$$

5.4 Conclusions

Vehicle rollover is more likely to occur on a banked surface. The threshold for wheel lift decreases with an increase in bank angle. The design of a dead-beat controller, however, is not affected by the bank angle. The controller needs to be recalculated only for new speeds because it is dependent only on speed and the constant parameters of the vehicle. For the scaled vehicle experiments, however, a different set of coordinates must be used and therefore a different roll model. The dead-beat controller is still designed using the same principle of replacing the undesired dynamics with those of a desired vehicle. The transfer functions must be formulated using the state-space representation in the error-fixed coordinates used to operate the scaled vehicle. In this chapter, a control algorithm was developed to mitigate rollover of the scaled vehicle on a banked surface by changing the dynamics of the system to those of an ideal vehicle that is less likely to experience rollover. The algorithm will be tested through experiment in the next chapter.

Chapter 6

Scaled Vehicle Implementation

In this chapter, the dead-beat controller method will be tested for effectiveness on the scaled vehicle. First, the scaled vehicle was operated at various conditions that induce wheel lift. Then a dead-beat controller was created to modify the steering input at those conditions. The effects of the filter were evaluated.

6.1 Wheel Lift in the Scaled Vehicle

Using the Penn State University Rolling Roadway Simulator (PURRS), the scaled vehicle can be operated under many different conditions. The scaled vehicle used is a 1/5 model of the Mercury Tracer. Table **6-1** shows a comparison of the dimensionless parameters for the scaled vehicle and Tracer as formulated during research on the PURRS. The parameters are relatively close in value. It is also interesting to note that a speed of 2.8 m/s for the scaled vehicle corresponds to a speed of 11.2 m/s for the Tracer. The dimensionless parameters ensure similar behavior, but the actual magnitudes of the dynamics may vary. The steering input can be chosen by selecting a lateral position input in the simulator. For this experiment, both a sinewave and a step input were used. The speed of the vehicle can also be adjusted by changing the speed of the treadmill. Finally, the treadmill can be rotated about the pitch and roll axes. Figure **6-1** is a picture of the PURRS.

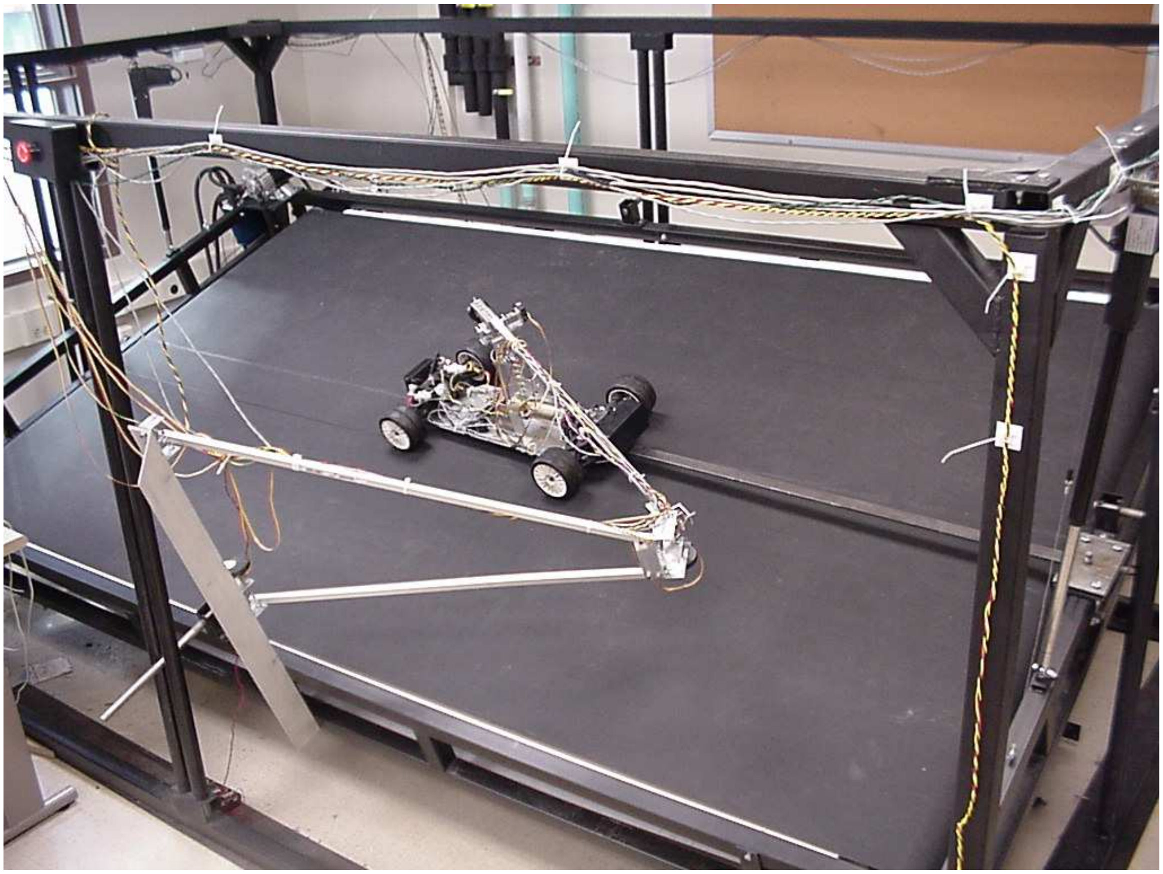

Figure **6-1**: Penn State University Rolling Roadway Simulator

6-1: Comparison of the Dimensionless Parameters for the Scaled Vehicle and the Mercury Tracer

Dimensionless Parameter	Scaled Vehicle	Mercury Tracer
Π_1	0.366	0.373
Π_2	0.634	0.626
Π_3	0.204	0.209
Π_4	0.563	0.562
Π_5	0.261	0.290
Π_6	0.038	0.059
Π_7	1.607	1.607
Π_8	2.230	1.710

Initially, aggressive step and sinewave inputs of multiple frequencies were used at speeds up to approximately 5.5 m/s while increasing the bank angle to approximately 25 degrees. The scaled vehicle did not experience wheel lift for any of these conditions. As seen in the previous chapter, the Tracer was not expected to experience wheel lift at high speeds or high bank angles. These results confirmed that the scaled vehicle did in fact have behavior similar to the Tracer, at least in regard to wheel lift propensity.

In order to test the control algorithm designed previously, the scaled vehicle needed to be modified such that wheel lift would occur. The CG height of the vehicle was increased by raising the mass attached to the front of the vehicle. Pictures of the vehicle before and after modifications are shown in Figure **6-2**. After modifications, the parameters of the vehicle were recalculated, and the modified parameters are listed in Table **6-2**. For comparison, the parameters of the original scaled vehicle are also listed. Note that unlike the creation of the High Roller, the overall mass of the scaled vehicle was not modified.

Table **6-2**: Modified Scaled Vehicle Parameters

Parameter	Modified Scale Vehicle	Scale Vehicle	Units
m	11.4	11.4	kg
ms	11.4	11.4	kg
Izz	1.2766	1.2766	kg-m^2
Ixx	0.4792	0.1843	kg-m^2
Ixz	0	0	kg-m^2
lf	0.240	0.240	m
lr	0.415	0.415	m
L	0.655	0.655	m
t	0.369	0.369	m
h	0.195	0.138	m
Cf	-219.59	-219.59	N/rad
Cr	-304.76	-304.76	N/rad
Kφ	239.12	239.12	N-m/rad
Dφ	11	11	N-s/rad

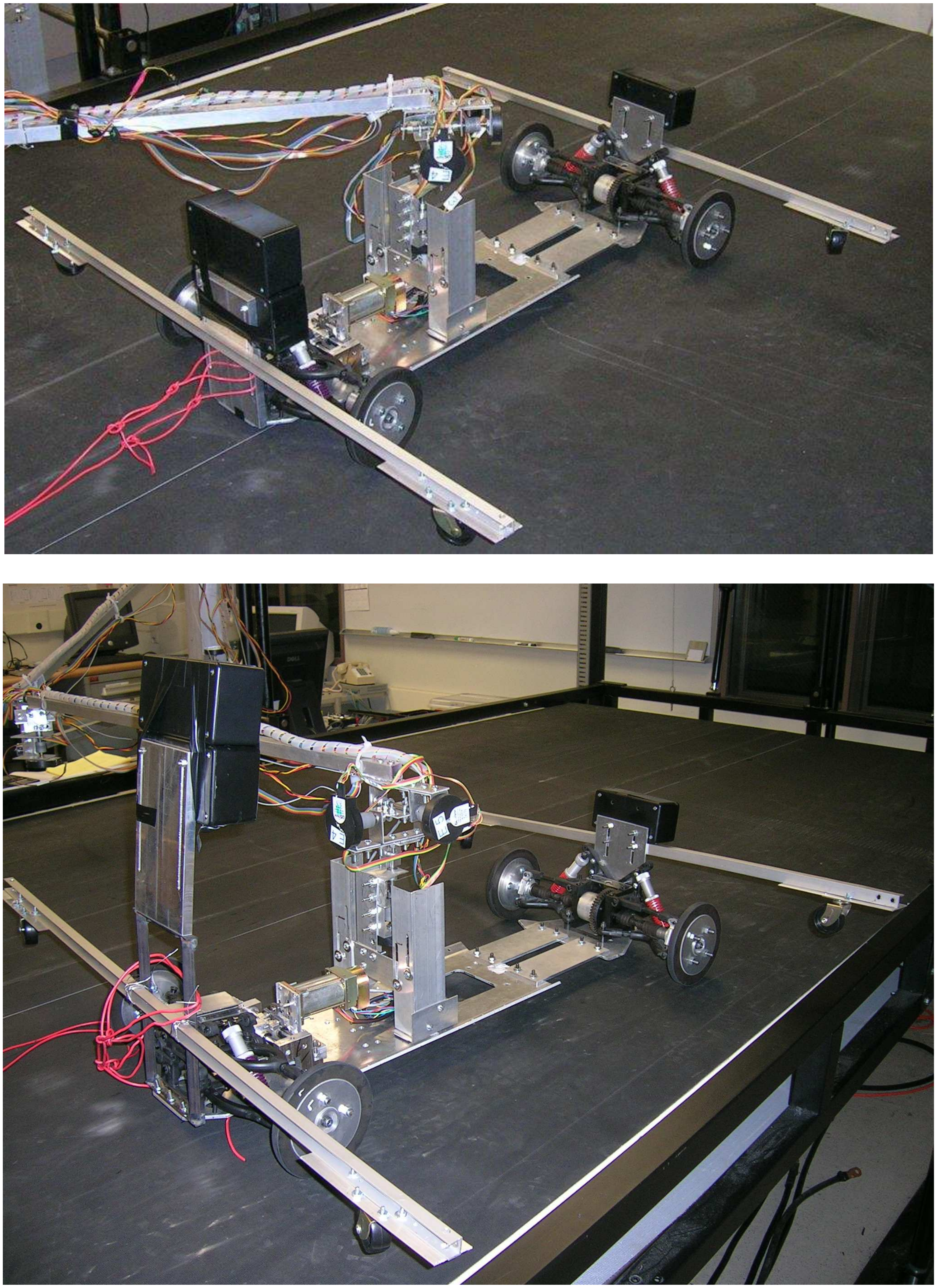

Figure **6-2**: Scaled Vehicle Before and After Raising the CG Height

After the modifications were complete, the scaled vehicle was placed on the treadmill for further experiment. An initial lateral position sinusoidal input of 0.6 Hz and amplitude of 0.1 m was selected based on previous data collected for the scaled vehicle which showed yaw rate instability near these areas. Furthermore, it was found that if the Tracer parameters were modified by increasing the height of its CG by the same amount with respect to the dimensionless parameters of the scaled vehicle, the Tracer would experience wheel lift at various speeds on a banked angle of 24 degrees. The wheel lift and tire slip thresholds are shown for the Tracer at a speed of 13.86 m/s in Figure **6-3**. Both the front and rear tires will experience wheel lift before slip for a range of input frequencies. It is interesting to note that the rear wheels are much more likely to experience wheel lift than tire saturation at these conditions.

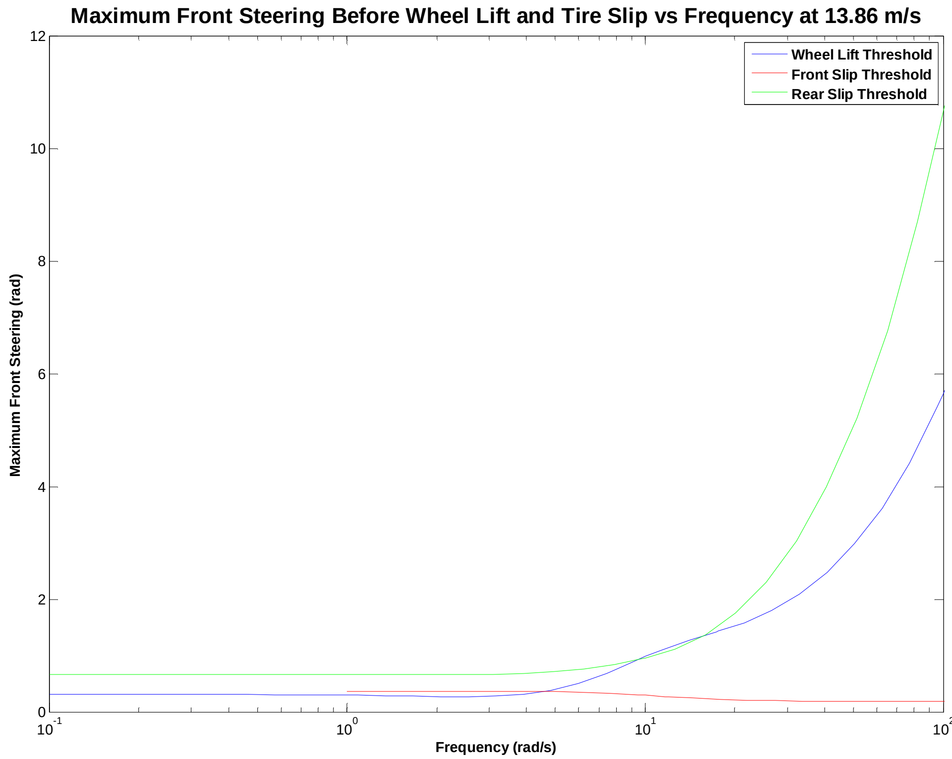

Figure **6-3**: Tracer with Raised Center of Gravity, Wheel Lift and Tire Saturation Thresholds on a Banked Angle of 24 Degrees at a Speed of 13.86 m/s

In the experiment, the bank angle of the treadmill was increased slowly along with the speed for the 0.6 Hz input. At a bank angle of approximately 24 degrees and a speed of 3.466 m/s, which corresponds to a speed of 13.86 m/s for the Tracer, the rear tires of the scaled vehicle began to experience wheel lift. The vehicle was then operated at the same speed and bank angle at a steering frequency of 0.9 Hz. The increase in frequency resulted in a larger roll angle and greater wheel lift. The frequency was then increased to 1.2 Hz. The vehicle also experienced wheel lift at these conditions, though the magnitude did not increase significantly.

Using the parameters of the modified scaled vehicle and the ideal vehicle from the previous chapter, a dead-beat control filter was designed for a speed of 3.466 m/s. The algorithm was then incorporated into the simulator to directly modify the steering input to the vehicle. At the same speed, bank angle, and frequencies the vehicle did not experience wheel lift. The control algorithm was successful in preventing the onset of rollover. The following figures show the recorded roll angle of the scaled vehicle at the various conditions with and without the implementation of the dead-beat controller. In all three cases, the roll angle of the vehicle is reduced significantly by the controller. The magnitude of the roll angle is decreased more at the higher frequencies. The algorithm appears to work exactly as expected.

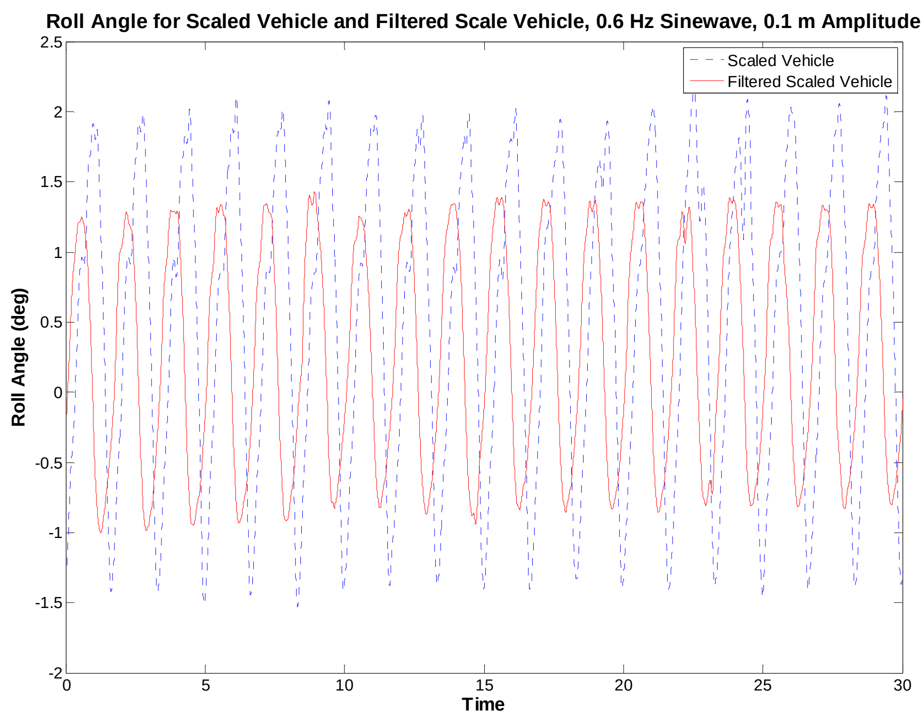

Figure **6-4**: Roll Angle of the Scaled Vehicle Reduced by the Filter at Speed of 3.466 m/s and Bank Angle of 24 degrees at Frequency 0.6 Hz

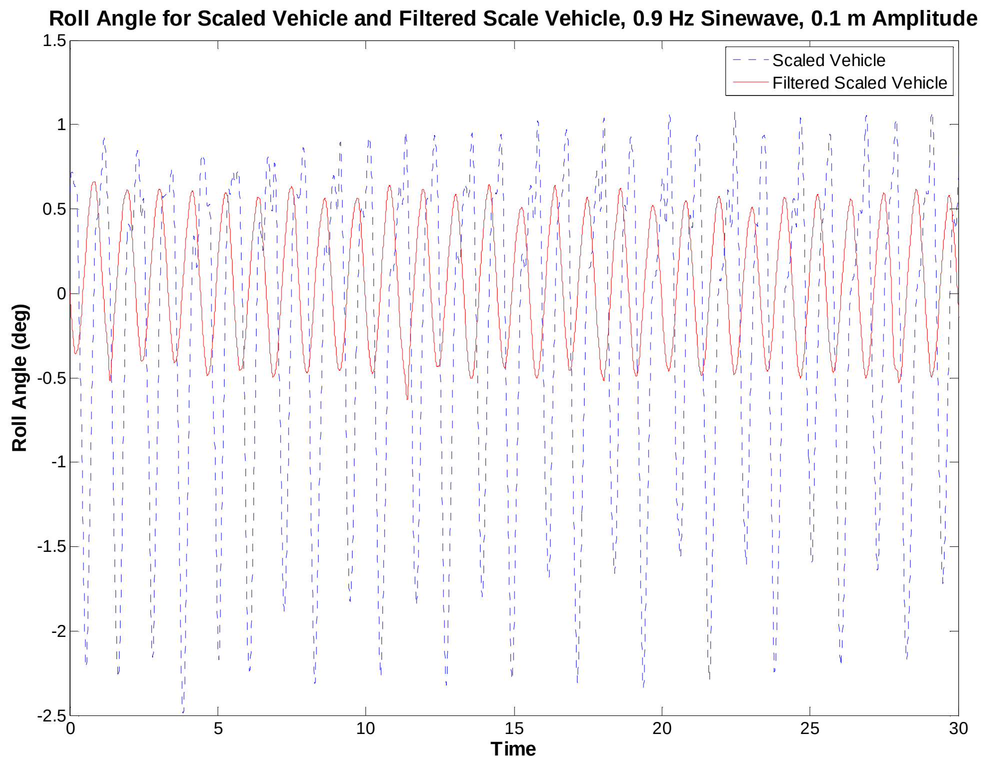

Figure **6-5**: Roll Angle of the Scaled Vehicle Reduced by the Filter at Speed of 3.466 m/s and Bank Angle of 24 degrees at Frequency 0.9 Hz

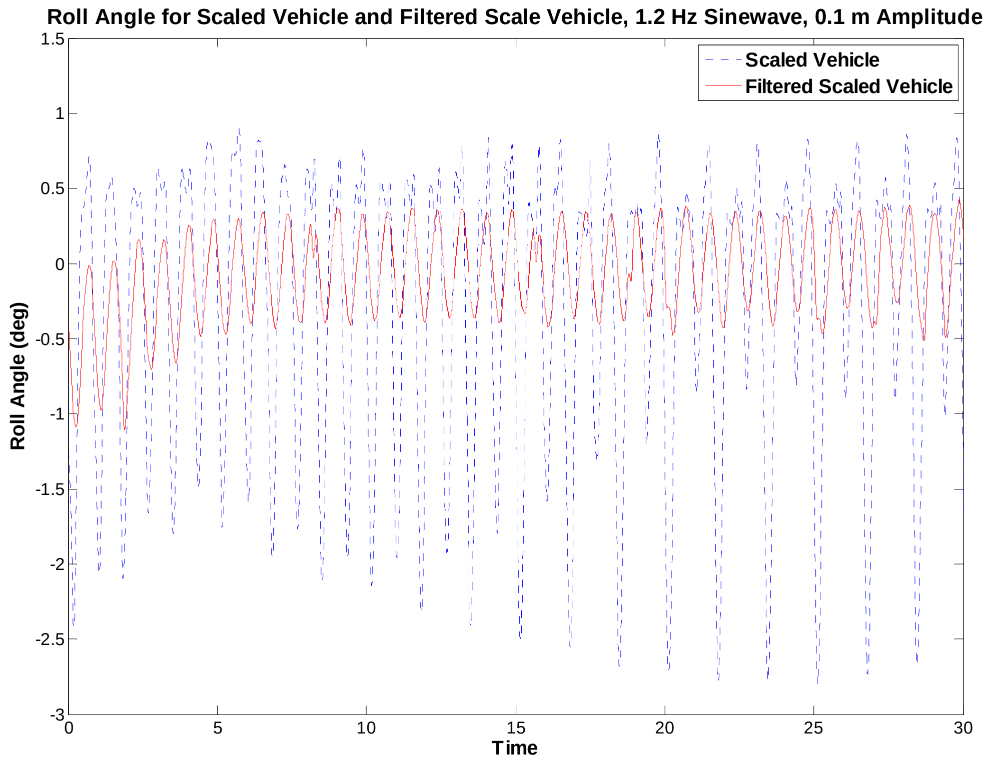

Figure **6-6**: Roll Angle of the Scaled Vehicle Reduced by the Filter at Speed of 3.466 m/s and Bank Angle of 24 degrees at Frequency 1.2 Hz

6.2 Conclusions

The scaled vehicle confirmed the results of the Tracer simulation and the effectiveness of the dead-beat controller. The scaled vehicle was unable to experience wheel lift at either sinewave or step inputs without modifying it parameters. Increasing the height of the CG, however, induced rollover. After wheel lift was achieved at various conditions, the dead-beat controller was used to modify the steering input to replace the unwanted dynamics with those of an ideal vehicle. Wheel lift no longer occurred at the same conditions while the controller was implemented. The controller appears to be a promising method for preventing wheel lift, and hence rollover.

Chapter 7

Conclusions

The conclusions of this thesis are organized as follows: conclusions regarding to the use of dynamic vehicle models to determine wheel lift thresholds, conclusions pertaining to feed-forward control as a method to prevent wheel lift, and conclusions relevant to the implementation of the dead-beat controller using the scaled vehicle. A discussion of future work pertinent to this thesis follows.

7.1 Determining Wheel Lift Thresholds Using Vehicle Dynamics

Before the conditions for wheel lift could be explored, vehicle dynamics must be understood. In this work, 2DOF and 3DOF models were used to study planar and roll motion respectively. The models largely agreed on their predictions for tire slip at various steering input frequencies. For the 3DOF model, the wheel lift threshold for vehicles was found to be related to the restoring moment of the suspension. If the maximum restoring moment is exceeded before tire saturation occurs, a vehicle may experience wheel lift and possibly rollover.

The effect of vehicle parameters pertaining to a vehicle's susceptibility to rollover were demonstrated by comparing the Mercury Tracer to its own High Roller version. Increasing the height of the center of gravity and decreasing the roll damping both increased propensity for wheel lift. It was also shown that rollover can be tripped by driving on a banked surface. As the angle of the banked surface increased, so did the propensity for wheel lift. Increasing the speed of the vehicle under the same conditions increased wheel lift susceptibility as well.

7.2 Using Feed-forward Control to Prevent Wheel Lift

To reduce wheel lift it is necessary to mitigate the dynamics that cause it. Decreasing the restoring moment of the suspension effectivley decreases the chance of rollover, and unsafe steering inputs can result in dangerous restoring moments. By modifying the steering input to prevent such hazardous conditions, the restoring moment can be reduced.

Feed-forward control was shown to be a simple way to directly change the input to the vehicle. In this work, dead-beat control was chosen for its simplicity, a technique that replaces the dynamics of an undesired system with those of a desired one. It was shown through simulation that the restoring moment could be decreased in magnitude by using this simple controller.

7.3 Scaled Vehicle Implementation

To demonstrate the ability of the dead-beat controller to change the dynamics of a vehicle to mitigate wheel lift, a scaled vehicle experiment was employed. The scaled vehicle was shown to have dimensionless parameters similar to those of the Tracer. Like the Tracer, the scaled vehicle was difficult to induce wheel lift for in an unmodified form.

By increasing the height of the center of gravity, however, the vehicle began to experience wheel lift when given a sinusoidal steering input on a banked surface. A similar modification of the Tracer parameters was simulated and it was shown that the Tracer would also experience wheel lift under similar conditions. Therefore, scaled vehicle testing proves to be a potential alternative to full-scale vehicle testing which can be extremely expensive and dangerous.

A dead-beat controller was then designed to help prevent rollover in the scaled vehicle. After implementation of the controller, the vehicle experienced a drastic reduction in roll angle and hence wheel lift. The controller was successful in preventing wheel lift under situations where the unmodified vehicle response clearly exhibited wheel lift.

7.4 Future Work

In further research, the scaled vehicle should be tested at many more conditions that produce wheel lift. Multiple bank angles, speeds, and alternate steering maneuvers should be incorporated in additional experiments. The controller should also be tested at conditions for which it was not specifically designed. In reality, the vehicle parameters may not be known accurately, and this may have a great effect on the viability of the controller. The dead-beat control method could also be compared to different algorithms to see if there is a more effective method that may not affect other dynamics of the vehicle. The possibility of negative effects on the dynamics exist and should be determined if so.

The ability of the scaled vehicle to accurately predict the roll dynamics of the full-scaled Tracer should also be explored. If the scaled vehicle method shows substantial evidence of its ability to foretell the behavior of the Tracer at various conditions, it may be used to confidently test the ability of various other algorithms to prevent rollover and other types of accidents. Parameters of the vehicle can easily be adjusted to simulate other vehicles as well. In addition, scaled vehicle testing may be able to replace or at least assist in full-scale vehicle testing. Scaled vehicle experimentation may help groups such as NHTSA determine what the worst case conditions for a vehicle are and consequently make their tests more effective in the process.

Further insight into the dynamic models used to describe vehicle behavior would also be beneficial. Other factors such as roll-steer and tire lag may need to be incorporated to fully depict the behavior of a vehicle. Future models may also wish to incorporate human factors. In an emergency situation, the reaction of the driver plays a large part in determining what input is given to the vehicle. As models of human-vehicle interaction become more accurate, the ability of the models to determine when undesired dynamics will occur under human input might also improve.